https://doi.org/10.5194/acp-2022-671
Preprint. Discussion started: 14 October 2022

Atmospheric Chemistry and Physics Discussions

Ground solar absorption observations of total column CO, CO_2, CH_4, and aerosol optical depth from California's Sequoia Lightning Complex Fire: Emission factors and modified combustion efficiency at large scales

Isis Frausto-Vicencio[1], Sajjan Heerah[2], Aaron G. Meyer[2], Harrison A. Parker[3], Manvendra Dubey[2] and Francesca M. Hopkins[1]

[1]Department of Environmental Sciences, University of California, Riverside, 92507, USA
[2]Los Alamos National Laboratory, Los Alamos, 87545, USA
[3]California Institute of Technology, Pasadena, 91125, USA

Correspondence to: Isis Frausto-Vicencio (ifrau001@ucr.edu)

Abstract. With global wildfires becoming more widespread and severe, tracking their emissions of greenhouse gases and air pollutants is becoming increasingly important. Wildfire emissions have primarily been characterized by *in situ* laboratory, and field observations at fine scales. While this approach captures the mechanisms relating emissions to combustion phase and fuel properties, their evaluation on large scale plumes has been limited. In this study, we report remote observations of total column trace gases and aerosols in the 2020 wildfire season of smoke plumes from the Sierra Nevada of California with an EM27/SUN solar Fourier transform infrared (FTIR) spectrometer. We derive total column aerosol optical depth (AOD), emission factors (EF) and modified combustion efficiency (MCE) for these fires, and evaluate relationships between them based on combustion phase at large scales. We demonstrate that the EM27/SUN effectively detects changes of CO, CO_2 and CH_4 in the atmospheric column at ~10 km scales that are attributed to wildfire emissions. These observations are used to derive total column EF_{CO} of 120.5 ± 12.2 and EF_{CH4} of 4.3 ± 0.8 for a large smoke plume event in mixed combustion phases. These values are consistent with *in situ* relationships measured in similar temperate coniferous forest wildfires. FTIR derived AOD was compared to a nearby AERONET station and observed ratios of AOD to X_{CO} were consistent with those previously observed from satellites. We also show that co-located X_{CO} observations from the TROPOMI satellite-based instrument are 9.7% higher than our EM27/SUN observations during the wildfire period. Finally, we put wildfire CH_4 emissions in context of the California state CH_4 budget and estimate that 213.7 ± 49.8 Gg CH_4 were emitted by large wildfires in California during 2020, about 13.6% of the total state CH_4 emissions in 2019. Our novel application of an EM27/SUN solar spectrometer to quantify wildfire emission ratios at large scales follows predictive relationships that are consistent with *in situ* studies, offering promise for extensive monitoring from ground networks and satellite remote sensing.

1 Introduction

Wildfires have become deadlier, more destructive, and more frequent globally over the past few years (UNEP, 2022). Particularly, the 2020 wildfire activity season surged with massive wildfires in the Western U.S., Australia, Brazil, and the Arctic. The California 2020 wildfire season was exacerbated by abnormally high temperatures and dry conditions (Jain et al.,

https://doi.org/10.5194/acp-2022-671
Preprint. Discussion started: 14 October 2022


Atmospheric Chemistry and Physics Discussions

2022; Cho et al., 2022) and emitted ten times more carbon dioxide (CO_2) into the atmosphere than the 2000-2019 annual average (California Wildfire Emission Estimates, 2021). Particulate matter 2.5 ($PM_{2.5}$) concentrations in the San Joaquin Valley (SJV), California were found to be four times higher during the 2020 fire season than non-fire periods (Ahangar et al., 2022). The high temperatures and dry conditions, combined with moisture from a tropical storm led to a dry lightning storm event in August, 2020, where lightning-ignited wildfires burned more acres in California than at any other time in recorded history (Morris III and Dennis, 2020). This included the lightning-sparked Castle Fire (part of the Sequoia Lightning Fire (SQF) Complex) that killed 10-14% of the large sequoias in the Sierra Nevada and has become the largest fire in a giant sequoia grove on record at 170,648 acres (Stephensen and Brigham, 2021). Historic fire suppression and land-use changes in this area has led to an increase of wildfires burning at higher intensity and larger areas (Moody 2006; Scholl 2010). Climate change has increased the forest fire activity in the Western U.S. (Zhuang et al., 2021) and will increase the likelihood for wildfires in the Sierra Nevada with greater burned area due to higher daily temperatures (Gutierrez et al., 2021), with implications for air quality and carbon emissions (Navarro et al., 2016).

Wildfires are a major source of air pollutants, including particulate matter (PM), carbon monoxide (CO), and greenhouse gases, primarily carbon dioxide (CO_2) and methane (CH_4) (Akagi et al., 2011; Wiedinmyer et al., 2011; Andreae, 2019). The high levels of PM and CO released from fires are dangerous to human health and degrade air quality on a local, regional, and global scale (Schneising et al., 2020; Aguilera et al., 2021). CO is an air toxic and is considered an indirect greenhouse gas as it is a major sink for the hydroxyl radical (OH), increasing the abundance of CH_4 through photochemical feedbacks (Li et al., 2018) and also produces ozone (O_3), a short lived greenhouse gas. CO_2 and CH_4 are the dominant greenhouse gases and are responsible for most of the current anthropogenic climate change (IPCC, 2014). A majority of carbon emissions from wildfires are of CO_2, CO, and CH_4 (~95%) while the remainder are carbonaceous aerosols (~5%) (Sommers et al., 2014; Urbanski, 2014). Although emissions from fires are biogenic sources of CO_2, they are released rapidly compared to the slow timescales of carbon uptake required to grow vegetation fuels. Increased fire activity increases atmospheric CO_2 in the short term, and can locally alter the terrestrial carbon cycle balance by reducing photosynthetic CO_2 uptake under high levels of vegetation disturbance (CARB, 2018). While CO_2 losses can be estimated as a function of burned area and fuel consumption, emissions of CO, CH_4, and aerosols are more difficult to estimate because they vary greatly with fire conditions. As global wildfires become more widespread and severe, tracking emissions of greenhouse gases and air pollutants from smoke will become increasingly important for efforts to track emissions of greenhouse gases and understand the impacts of fire on the atmosphere (Aguilera et al., 2021; Wilmot et al., 2022).

Our understanding of the atmospheric impacts of increasing fire activity relies on accurate observations and process-based estimation of fire emissions that have been developed using *in situ* measurements (Urbanski, 2014). While several space-based instruments can retrieve and derive emissions of important trace gases globally, observations are limited by spatiotemporal coverage and focus on aerosol burden from smoke plumes with limited attention to trace gases, and a lack of integration of trace gases and aerosols. Ground-based solar spectrometers present a new technique to measure and understand fire emissions at regional scales, and temporally complement satellite observations. Column measurements are insensitive to

https://doi.org/10.5194/acp-2022-671
Preprint. Discussion started: 14 October 2022


Atmospheric Chemistry and Physics Discussions

the planetary boundary layer growth and are less affected by nearby point sources than *in situ* measurements, making them a good candidate for regional-scale monitoring (Lindenmaier et al., 2014). The EM27/SUN is a ground-based remote sensing instrument that is relatively portable and robust for field deployments. These instruments are the basis for the ground-based network of FTIR COCCON (COllaborative Carbon Column Observing Network), which complements NDACC (Network for the Detection of Atmospheric Composition Change) and TCCON (Total Column Carbon Observing Network), two high resolution FTIR trace gas monitoring networks (Frey et al., 2019; Wunch et al., 2011; Toon et al., 2009; De Mazière et al., 2018).

Field-based measurements of biomass burning in temperate forests are limited and sparse (Burling et al., 2011; Urbanski, 2014), despite the increase in burning activity in the Western U.S. (Zhuang et al., 2021). The EM27/SUN provides vertically integrated column measurements of CH_4, CO_2, and CO which allows for calculating modified combustion efficiency (MCE) and emission factors (EF) in the total column of smoke plumes downwind of wildfires. MCE values give insight into the relative amounts of flaming and smoldering combustion of the fire. Pure flaming combustion has an MCE of 0.99, while the MCE for smoldering varies from 0.65 to 0.85. A value near 0.90 indicates equal contributions of flaming and smoldering combustion (Akagi et al., 2011). EF are defined as the mass of gas or aerosol emitted per dry biomass consumed and are critical inputs for models to accurately calculate emissions and construct wildfire inventories (Urbanski, 2014). Providing new EFs will help improve regional biomass burning estimates. Past studies have derived atmospheric column-based EFs with respect to CO from wildfires using solar FTIR spectrometers (Kille et al., 2022; Paton-Walsh et al., 2005; Lutsch et al., 2020, 2016; Viatte et al., 2014, 2015). The observed small changes in CO_2 with respect to the large atmospheric background has limited previous FTIR-based studies in their ability to derive EFs with respect to CO_2. This has consequently inhibited the calculation of MCE. Here, we present the first EFs with respect to CO_2 and MCE for wildfires calculated by total-column FTIR.

During part of the 2020 wildfire season, we deployed the EM27/SUN in the SJV downwind of two major wildfires, the Creek Fire and Sequoia Lightning Fire (SQF) Complex, in the Sierra Nevada. We report $EF_{CO/CO2}$ and $EF_{CH4/CO2}$ from the SQF Complex, a mixed conifer forest wildfire in the Sierra Nevada, and follow the wildfire's combustion phases with MCE values. Furthermore, because ground-based column measurements operate on similar scales as satellites and regional atmospheric models (McKain et al., 2015), we compared EM27/SUN measurements with satellite greenhouse gas observations from TROPOMI collected during the fires. We quantify MCE, EF for CO_2 and CH_4, and AOD enhancements from the SQF using EM27, we compare CO retrievals to TROPOMI, we compare AOD retrieval to an AERONET site, and we put wildfire CH_4 emissions in context of the California state CH_4 budget. Our work demonstrates a novel application of the ground based EM27/SUN solar spectrometers in wildfire monitoring and contributes to the development of techniques for analyzing remotely sensed greenhouse gas measurements.

2 Data Sources and Methods

2.1 EM27/SUN Atmospheric Column Observations

https://doi.org/10.5194/acp-2022-671
Preprint. Discussion started: 14 October 2022


Atmospheric Chemistry and Physics Discussions

We measured the column-averaged dry air mole fractions (X_{gas}) of CH_4, CO_2 and CO (X_{CH4}, X_{CO2}, and X_{CO}) in a location 60 km west of the SQF Complex (Castle and Shotgun fires) and 80 km southwest of the Creek wildfires in the Sierra Nevada, and southeast of major dairy farms in the SJV (Figure 1, panel a). The SQF Complex fires began on Aug. 19 after a dry thunderstorm and lightning event ignited the fires in the Sierra Nevada. By Sept. 12, the SQF Complex had grown to 283 km^2. The Creek fire began on the evening of Sept. 5 and upper-level high winds produced a pyro-cumulus cloud on Sept. 6 that reached an altitude over 15 km (Morris III and Dennis, 2020). Smoke filled the valley and smoky overcast skies remained in large parts of the SJV for the next two weeks as fires kept burning. In total, the SQF Complex consumed 686 km^2 and Creek consumed 1515 km^2, placing both these fires among the top 20 largest California wildfires (Morris III and Dennis, 2020).

The Bruker Optics EM27/SUN solar-viewing Fourier Transform Spectrometer owned by Los Alamos National Laboratory (LANL) collected continuous daytime column measurements in Farmersville, California (36.31, -119.19) from Sept. 8 until Oct. 17, 2020, for a total of 40 days of observations. The EM27/SUN solar spectrometer has been previously used to study emissions from urban and agriculture CH_4 and CO_2 sources (Chen et al., 2016; Viatte et al., 2017; Dietrich et al., 2021; Alberti et al., 2022a; Makarova et al., 2021; Heerah et al., 2021). The recent addition of a CO detector in Bruker's EM27/SUN Fourier Transform Infrared (FTIR) spectrometer increases the instrument's utility for measuring combustion sources and as a validation tool for TROPOMI column X_{CO} as it covers the same spectral region (Hase et al., 2016). The EM27/SUN uses the sun as the light source which allows it to derive aerosol optical depth (AOD) as demonstrated by Barreto et al. (2020) at the TCCON FTIR and AERONET site at Izaña, Spain. In their study, TCCON spectra were degraded to the same resolution as the EM27/SUN (0.5 cm^{-1}) and they concluded that EM27/SUN spectra would be able to effectively derive AOD. Following their approach, we derive AOD for the wildfire period from our measurements. Further details of the AOD calculation are found in Section 2.4.

EM27/SUN X_{gas} values were retrieved from unaveraged double sided interferograms using the I2S and GFIT (GGG2014 version; https://tccon-wiki.caltech.edu/) retrieval algorithms automated by the EGI processing suite (Hedelius et al., 2016). Surface pressure is required to retrieve dry air columns in GGG and we used Coastal Environmental Systems ZENO weather station to record surface pressure at our field site for retrievals. Retrievals also require atmospheric profiles of temperature, pressure, altitude and water and these profiles were extracted from NCEP/NCAR reanalysis product (Kalnay et al., 1996). We calibrated the EM27/SUN via co-located measurements alongside the IFS125, a high-spectral-resolution FTIR operated by TCCON at the California Institute of Technology (CIT), both before and after the collection periods to determine calibration factors (R_{gas}) assuming a linear model forced through the origin for each gas, e.g., $X_{TCCON} = X_{EM27}\, R_{gas}$ (Chen et al., 2016; Hedelius et al., 2016). The TCCON network sets the standard as the current state-of the art ground-based validation system for remote sensing and satellite-based observations of greenhouse gases (Wunch et al., 2011), and TCCON observations are tied to the World Meteorological Organization (WMO) standard greenhouse gas scale. Co-locating the EM27/SUN and TCCON instruments ensures system stability of the EM27/SUN after transportation to field sites. Co-located measurements were performed on Sept. 2–3, 2020 and Oct. 30–Nov. 1, 2020. Results of the correction factors from the co-located measurements are shown in Table A1 of the Appendix. The TCCON instrument also uses the GFIT retrieval algorithm with

https://doi.org/10.5194/acp-2022-671
Preprint. Discussion started: 14 October 2022

Atmospheric Chemistry and Physics Discussions

the same *a priori* profiles; however, due to different instrument spectral resolutions and averaging kernels, we correct for the differences between the EM27/SUN and TCCON instrument following Hedelius et al., 2016 (Equation A4) to adjust the EM27/SUN retrievals before comparing with TCCON and deriving calibration factors.

Prior to measurements in California, the EM27/SUN was stationed in Fairbanks, Alaska for several months. Given the different settings used with the CamTracker, the solar disk was not centered on the camera and this misalignment was found on Sept. 7. Based on co-located measurements with the CIT TCCON on Sept. 2 and 3, it was determined that the observations within the second detector of X_{CO} were affected on the days prior when camera was misaligned (Sept. 2, 3, 6, and 7). For this reason, we report measurements of X_{CO}, X_{CO2} and X_{CH4} beginning on Sept. 8 and use the Oct. 30 – Nov. 1 co-located measurements for calculating correction factors. AOD was derived from micro windows within the first detector, thus calculations of AOD were not affected.

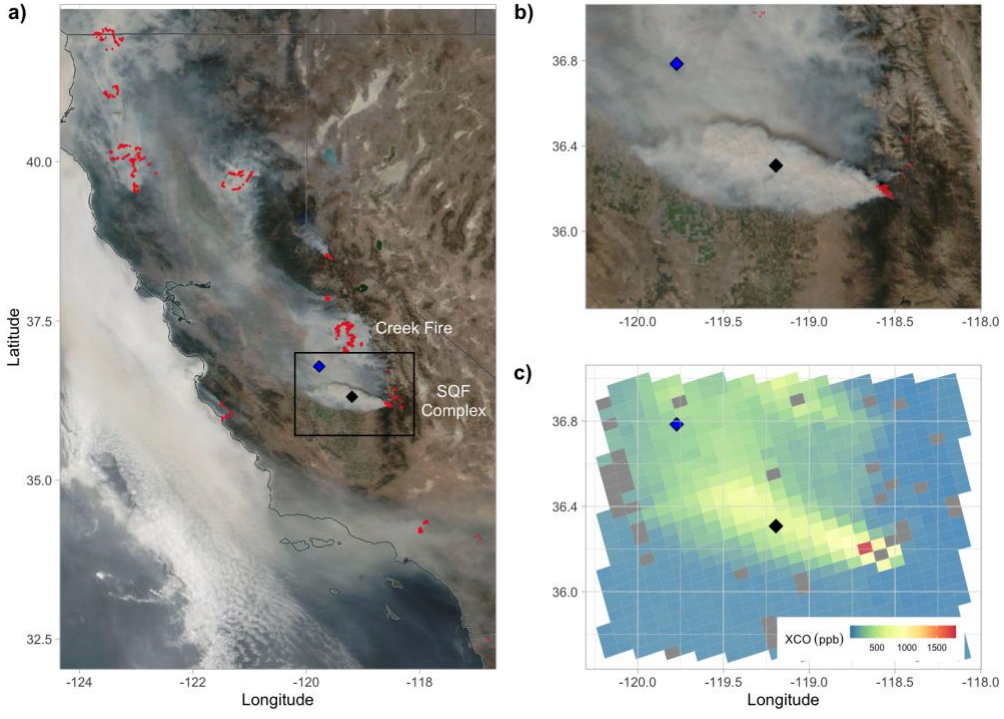

Figure 1. a) Satellite imagery captured by NOAA-20 VIIRS of heavy smoke in California on September 12, 2020, highlighting fire and thermal anomalies in red (NASA Worldview; worldview.earthdata.nasa.gov), and with black diamond shape showing the EM27 measurement location and blue diamond shape the AERONET observational site. b) Inset shows more detail of the smoke plume within the SJV from the SQF Complex in the Sierra Nevada, shown by red thermal anomalies at the right of the image. c) Inset of TROPOMI XCO overpass at 2020-09-12 13:54 PDT.

https://doi.org/10.5194/acp-2022-671
Preprint. Discussion started: 14 October 2022


Atmospheric Chemistry and Physics Discussions

2.2 TROPOMI CO Column Measurements

TROPOMI is an instrument launched in late 2017 onboard the European Space Agency's (ESA) Sentinel-5-Precursor (S5P). The instrument measures Earth radiance spectra in the ultraviolet (UV), NIR and SWIR allowing for measurements of a wide range of atmospheric trace gases and aerosol properties (Veefkind et al., 2012). The satellite has a sun-synchronous orbit with daily global coverage and a spatial resolution of 5.5 x 7 km^2 for CH_4 and CO operational level 2 (L2) products. The offline (OFFL) CO total column L2 data product filtered for quality assurance values > 0.5 are used in this work as recommended in the product readme file (https://sentinel.esa.int/documents/247904/3541451/Sentinel-5P-Carbon-Monoxide-Level-2-Product-Readme-File, last access: 4 Aug 2022). This selection filters out high solar zenith angles, any corrupted retrievals, and influences from high clouds. The majority of the TROPOMI X_{CH4} product was flagged out near the observational site during our measurement period, and hence was not included in this analysis. Following Sha et al., 2021, the TROPOMI CO column densities were converted to X_{CO} (ppb) by using the modeled surface pressure and total column of H_2O to calculate the column of dry air.

We evaluated the agreement between the retrieved X_{CO} from EM27/SUN and TROPOMI overpasses during the measurement period. This allows for a novel evaluation of the TROPOMI sensor under wildfire conditions of high X_{CO} and aerosol loading in the atmosphere. A correction factor was calculated to account for differences in the *a priori* profile used in the retrieval of X_{CO} in both instruments. We follow the *a priori* substitution method described in (Sha et al., 2021; Jacobs, 2021) to calculate an additive factor for the EM27/SUN. Due to the possibility of measuring narrow smoke plumes on subgrid spatiotemporal scales, we perform a sensitivity study to determine the best co-location criteria for the EM27/SUN to TROPOMI comparison by varying the maximum radius (5 – 50 km) from the observational site and averaging time (5 – 30 min) for the EM27/SUN measurements around the TROPOMI overpass time. We require a minimum threshold of at least three 1-minute averages within the averaging time aggregations.

2.3 AERONET Data

AERONET (http://aeronet.gsfc.nasa.gov/ accessed on 15 June 2022) is a global network of sun/sky radiometer with over 600 sites operated around the globe. AERONET observations include measurements of aerosol optical depth, microphysical and radiative properties. The stations are frequently calibrated, and they set the standard for aerosol measurements and validation for satellite products. AERONET measures AOD at several spectral windows from 340, 380, 440, 500, 675, 870, 940, 1020 and 1640 nm. The Ångström exponent (AE), describing the wavelength dependence of aerosol optical thickness, is calculated from the spectral AOD. We used the AERONET Level 2.0 version 3 AOD and AE data from the Fresno_2 site (36.78, -119.77) that has been operating in the same location since 2012. This site is located about 90 km away from our EM27/SUN site. Further quality control information can be found in Giles et al., 2019.

https://doi.org/10.5194/acp-2022-671
Preprint. Discussion started: 14 October 2022


Atmospheric Chemistry and Physics Discussions

2.4 AOD Calculation

To calculate AOD from the EM27/SUN solar measurements, we follow the methods described in Barreto et al. (2020) who found good agreement between AERONET and TCCON FTIR-derived AOD at the high altitude Izaña Observatory in Spain. Their analysis was performed on degraded TCCON FTIR solar spectra (0.5 cm^{-1}) to assess the capability of lower resolution FTIR EM27/SUN instruments to detect broadband aerosol signal. Ten interferogram scans were co-added to increase the signal to noise ratio of the aerosol retrieval for a total integration time of 1 minute. We calculated AOD from four recommended micro windows with high solar transmission centered at 1020.9, 1238.25, 1558.25, and 1636 nm and compare to a nearby AERONET site located in Fresno, CA.

We apply the methods further described in Barreto et al. (2020) that are based on the Beer-Lambert-Bougher attenuation law:

$$V_\lambda = V_{o,\lambda} \cdot d^{-2} \cdot \exp(-m \cdot \tau_\lambda) \quad (1)$$

where V_λ is the measured solar irradiance at wavelength λ, $V_{o,\lambda}$ is the spectral irradiance outside the Earth's atmosphere at wavelength λ, d is the ratio of mean to actual sun-earth distance, and m is the optical air mass (Kasten and Young 1989). The V_o is derived from the Langley method by utilizing the measured solar intensity (V) versus the optical air mass (m) and extrapolating to an optical air mass of zero. The total optical depth (τ_λ) is the sum of the optical depth of Rayleigh scattering ($\tau_{R,\lambda}$), gas absorption ($\tau_{g,\lambda}$), and aerosols ($\tau_{a,\lambda}$):

$$\tau_\lambda = \tau_{R,\lambda} + \tau_{g,\lambda} + \tau_{a,\lambda}. \quad (2)$$

Barreto et al. (2020) carefully selected and evaluated several FTIR micro windows to minimize the gas absorption, thus $\tau_{g,\lambda}$ is considered negligible. Rayleigh scattering is calculated following Bodhaine et al. (1999) using the pressure measured at the measurement site by the ZENO weather station. The AOD $\tau_{a,\lambda}$ can then be calculated by subtracting Rayleigh scattering from the equation below:

$$\tau_{a,\lambda} = \frac{\ln(V_{o,\lambda} \cdot d^{-2}\cdot) - \ln(V_\lambda)}{m} - \tau_{R,\lambda}\,. \quad (3)$$

A cloud filter is applied to the spectra based on the measured fractional variation in solar intensity (fvsi). We set this quality filter to a maximum of 0.5% variability to ensure minimum cloud interference. The optical air mass range for Langley plot calibrations were performed from $1.5 \leq m < 7$ to avoid large errors at smaller air masses and turbidity influence at solar noon. A plot of ln(Vo) is found in Appendix B, Figure B1 displaying the calculated ln(Vo) over time from September to

https://doi.org/10.5194/acp-2022-671
Preprint. Discussion started: 14 October 2022


Atmospheric Chemistry and Physics Discussions

November 2020. Mirror degradation and exposure to dust or ash from fires can be observed in a declining ln(Vo) and a sudden jump in ln(Vo) is observed in late October and early November after the mirrors were cleaned, suggesting that debris had diminished the solar intensity measured by the FTIR instrument. Due to the varying ln(Vo), we calculate AOD only for the first week of data collection (Sept. 8 – 15) using the ln(Vo) obtained during the earlier period of September, summarized in Table B1 of Appendix B.

A time series of the FTIR-derived AOD for the four micro windows is shown in Figure B2 of Appendix B where a spectral dependance of the aerosol absorption can be observed in the plot with longer wavelengths recording smaller AOD. Although our FTIR-derived AOD is limited to the spectral range from the FTIR detector (1020.9 – 1636 nm), we used the Ångström exponent to derive FTIR AOD at 500 nm to enable a comparison with other studies shown in Figure 4. A plot of AOD at 1020.9 and 1636 nm with AERONET at 1020 and 1640 nm can be found in the Appendix B, Figure B3.

2.5 Estimating Emission Factors and Modified Combustion Efficiency

We demonstrate the capability of ground-based solar column measurements to calculate important variables for fire research including EFs and MCE for determining fire emissions and understanding different combustion phases of wildfires. As a case study, Sept. 12 observations were selected as this day had the highest observed X_{CO} and dominant influence from the SQF Complex (Figure 1b). We estimate emission ratios of CH_4 and CO ($ER_{CH4/CO2}$ and $ER_{CO/CO2}$) by calculating the slope from a York linear regression of CO and CH_4 excess mole fractions (ΔX_{CO} and ΔX_{CH4}) relative to CO_2.

$$ER_X = \frac{\Delta X}{\Delta CO_2} = \frac{X_{Fire} - X_{Background}}{CO_{2\,Fire} - CO_{2\,Background}}. \quad (4)$$

Emission factors ($EF_{CH4/CO2}$ and $EF_{CO/CO2}$) were then calculated as shown in equation 5 by multiplying the ER by the molar mass of either CO or CH_4 (MM_X), divided by the molar mass of carbon (MM_C), and total carbon emitted (C_T) while assuming 500 ± 50g C is emitted per kilogram of dry biomass consumed ($M_{Biomass}$) (Akagi et al., 2011; Burling et al., 2010). C_T is given by Equation 6, where n is the number of carbon-containing species measured, Nj is the number of carbon atoms in species j, and ΔCj is the excess mixing ratio of species j (Yokelson et al., 1999).

$$EF_X = \frac{ER_X}{C_T} * \frac{MM_X}{MM_C} * M_{Biomass} \quad (5)$$

$$C_T = \sum_{j=1}^{n} N_j \times \frac{\Delta C_j}{\Delta CO_2} \quad (6)$$

The MCE is commonly used as a relative measure between the smoldering and flaming combustion phases. Smoldering emissions have an MCE from 0.65-0.85, pure flaming emissions have an MCE of 0.99 and emissions near 0.9 have roughly

https://doi.org/10.5194/acp-2022-671
Preprint. Discussion started: 14 October 2022


Atmospheric Chemistry and Physics Discussions

equal amounts of flaming and smoldering combustion (Akagi et al., 2011). MCE was calculated by dividing excess mole fraction of CO_2 (ΔCO_2) by the total excess mole fraction of CO and CO_2:

$$MCE = \frac{\Delta CO_2}{\Delta CO + \Delta CO_2}. \quad (7)$$

Due to averaging kernel differences across the trace gases, an averaging kernel correction is applied to Equations 4 and 7, see Appendix C. The enhancement over background mixing ratios (ΔX_{gas}) for each measurement day was calculated by subtracting the background ($X_{gas,\ bkdg}$) determined as the 2nd percentile of daily measured mixing ratios (X_{gas}). A sensitivity test showed that emission ratios did not significantly change if background was calculated using 1st-5th percentiles. The monthly background in September was 411.3 ppm for X_{CO2}, 99.4 ppb for X_{CO} and 1905.3 ppb for X_{CH4}. The monthly average mixing ratios measured *in situ* at Mauna Loa for CO_2 were 411.5 ± 0.2 ppm and CH_4 1884.7 ± 1 ppb during September 2020 (https://gml.noaa.gov/obop/mlo/).

3 Results

3.1 Observations X_{CO}, X_{CO2}, and X_{CH4} from wildfires in the San Joaquin Valley

The first week of trace gas measurements are shown in Figure 2 in addition to the daytime fire radiative power (FRP), an indicator of fire intensity measured by VIIRS Active Fire and Thermal Anomalies product from NOAA-20. Fire-emitted CO can be observed in the timeseries and X_{CO} is exceptionally high on Sept. 12, reaching mixing ratios 10 times higher than the previous days. A large smoke plume was captured by the NOAA VIIRS satellite on Sept. 12 originating from the SQF Complex and traveling west directly over the measurement site as seen in Figure 1b. Sept. 12 also corresponds to the highest FRP during this record. The next day, Sept. 13, both fires remained active; however, their smoke plumes were transported northward as reflected by a lower X_{CO} in our observations relative to Sept. 12.

X_{CO2} and X_{CH4} were also enhanced on the Sept. 12 smoke event and followed the same trend as X_{CO} over the course of the day. Over 30 dairy farms are located northwest of the measurement site and they are expected to influence observed X_{CH4} and X_{CO2}; dairy influence is notable on days with predominantly westerly winds (e.g. Sept. 8 and 11). X_{CO}, X_{CO2}, and X_{CH4} averaged at 154 ± 78 ppb, 413 ± 1 ppm, and 1938 ± 27 ppb from Sept. 8 to Oct. 17. X_{CO} and X_{CO2} peaked on Sept. 12 at 1012.8 ppb and 421.6 ppm, while X_{CH4} peaked on Sept. 28 at 2050.1 ppm due to dairy farms in the area. The measured X_{CO} on Sept. 12, 2020, is the highest reported X_{CO} value in EM27/SUN literature. Retrievals of X_{gas} using the EM27 in such dense smoke plume has not been reported in previous studies. Using this date as a case study, we calculate total column EF and MCE to study the evolution of the fire over the course of the day further described in Section 3.4. We isolate the Sept. 12 fire smoke plume by taking the X_{CO} mixing ratios that exceeded the 98th percentile (>335.1 ppb) from all observations over our

https://doi.org/10.5194/acp-2022-671
Preprint. Discussion started: 14 October 2022

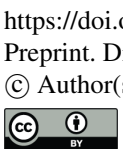

Atmospheric Chemistry and Physics Discussions

measurement period. This period corresponded to mixing ratios recorded after 12:00 pm when X_{CO} and X_{CO2} began to increase considerably.

The time since emission of the observed smoke plume was estimated to be ~1.5 hr. This was calculated by dividing the distance away from the SQF Complex fire (~60 km) by the average wind speed (11.2 ± 0.8 m/s) at the height of the smoke plume (4.1 ± 1.2 km). The height of the plume was determined by taking a mean of the available pixels within the smoke plume of aerosol layer height product from TROPOMI (http://www.tropomi.eu/data-products/aerosol-layer-height). The mean wind speed measured at 4.1 ± 1.2 km came from a 915 MHz Wind Profiler located in Visalia, CA about 20 km west of the observational site (data available at: ftp://ftp1.psl.noaa.gov/psd2/data/realtime/Radar915/).

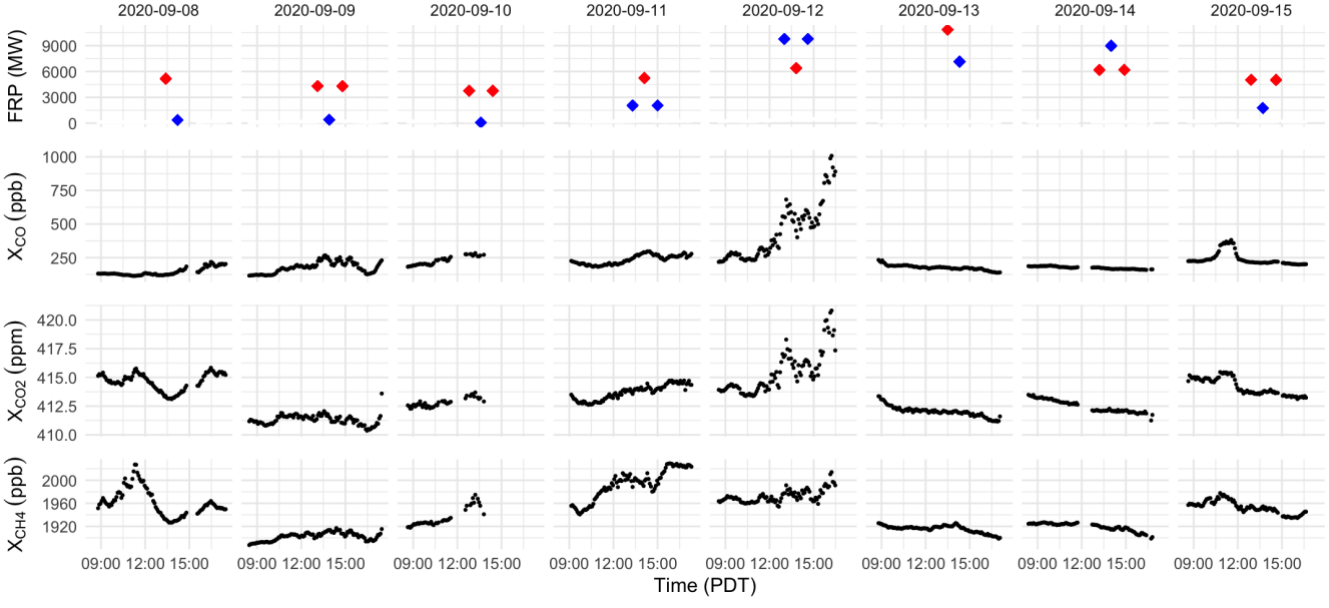

Figure 2. Timeseries of daytime total FRP from VIIRS NOAA-20 of Creek fire (red) and SQF Complex (blue) and of 5-minute mean observations from the ground-based EM27/SUN solar-viewing spectrometer during the first week of measurements September 8 – 15, 2020.

3.2 Comparison of EM27/SUN and TROPOMI retrievals

In this section, we compare X_{CO} retrieved from ground-based EM27/SUN observations downwind of the Sierra Nevada wildfires to satellite-based X_{CO} retrievals from coincident TROPOMI overpasses. Previous studies of X_{CO} and X_{CH4} comparisons between TROPOMI and EM27/SUN's have used a TROPOMI soundings between 50 – 100 km from the observational site and used EM27/SUN measurements between 40 mins – 1 hour TROPOMI overpass as a coincident criteria (Sha et al., 2021; Jacobs, 2021; Sagar et al., 2022; Alberti et al., 2022b). Given the spatial and temporal heterogeneity in smoke plumes from wildfires observed in Figure 1 and Figure 2, we perform a sensitivity study of different radii (10, 15, 20, 30, 40,

https://doi.org/10.5194/acp-2022-671
Preprint. Discussion started: 14 October 2022

Atmospheric Chemistry and Physics Discussions

50 km) from our observational site and time averages (10, 15, 20, 30 mins) to determine adequate criteria for comparison during a wildfire event. An illustration of the sensitivity analysis is shown in Figure D1, Appendix D.

We quantify the sensitivity of different TROPOMI radii and averaging times in comparison with our EM27/SUN data by calculating the mean difference, mean relative difference and R^2 between the linear regression fits for the measurements. We find that all combinations produce a positive mean bias, meaning that TROPOMI overestimates X_{CO} compared to the EM27 measurements. TROPOMI pixels within a radius of 5 km averaged with 30-minute aggregations of EM27/SUN gives the lowest mean difference of 10.64 ppb, mean relative difference of 5.5%, and highest correlation coefficient of 0.99, however, only 4 points coincide during the measurement period. To maximize the number of coincidences while maintaining a low bias, we select 15 km as the maximum radius with a 30-minute averaging time. This gives a total of 19 coincident data points and mean difference of 17.2 ppb, mean relative difference of 9.7%, and R^2 of 0.97. A timeseries of the coinciding data pairs from the EM27/SUN 30-minute average observation period with TROPOMI overpass with a 15 km radii are shown in Figure 3a and the correlations are shown in Figure 3b. Applying these spatial and temporal criteria results in large variance for the largest measured X_{CO} due to heterogeneity in the smoke plume event. The EM27/SUN displays a larger variance than TROPOMI due to capturing the 30-minute temporal variability in the plume as it was transported above the instrument. We find a strong correlation between CO column averages with an R^2 of 0.97 and a York linear regression fit of y = 1.36x – 40.15. These results suggest an overestimation of 9.7% X_{CO} from TROPOMI observations of wildfires.

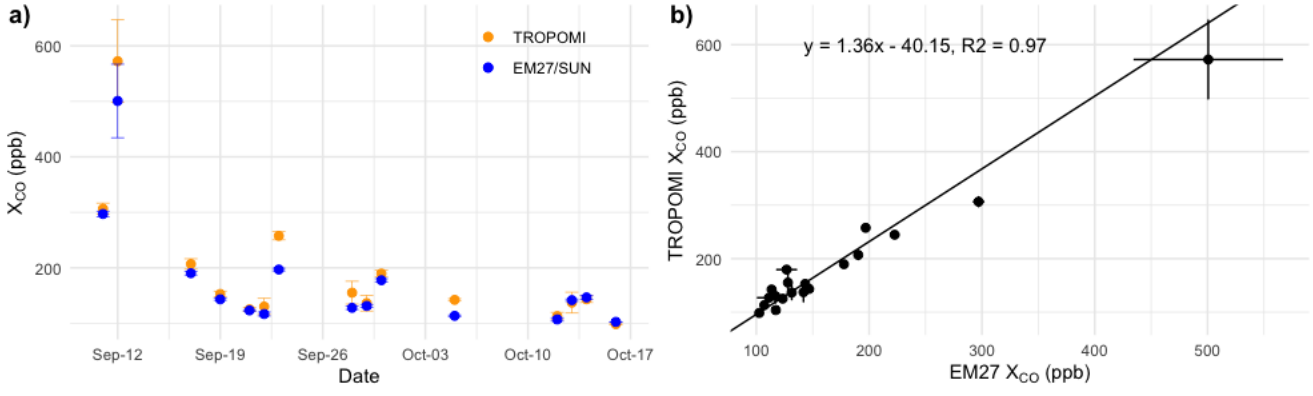

Figure 3. a) Timeseries of coinciding EM27/SUN 30-minute average observation period with TROPOMI overpass with 15 km radius. b) Correlation between coinciding TROPOMI and EM27/SUN data pairs. The error bars are the standard deviation of the TROPOMI averaged pixels at 15 km and EM27/SUN 30-minute observation.

3.3 Aerosol optical depth derived from measured solar intensity

We show a timeseries of AOD at 500 nm derived for the first week of measurements in Figure 4 (Sept. 8 – 15) plotted with AOD at 500 nm from an AERONET station in Fresno (Sept. 4 – 19), about 90 km north of the measurement site (Figure 1). Similar to observations of X_{CO}, enhancements of AOD are observed through the week with the highest recorded AOD on

https://doi.org/10.5194/acp-2022-671
Preprint. Discussion started: 14 October 2022

Atmospheric Chemistry and Physics Discussions

Sept. 12. The observational sites were relatively far from each other (~90 km) and although smoke reaching the two sites varied over these spatial scales, the FTIR AOD follows the same inter-day trend as the AOD measured by the AERONET with a peak in AOD on the 12th. Intraday variability between the sites do not seem to follow the same trend. This suggests that the EM27/SUN AOD estimate was also able to qualitatively capture the increase in aerosols in the SJV as fires burned more intensely and smoke from fires moved into the valley due to synoptic conditions. Differences are observed in the AOD timeseries as these two sites were downwind of two different fires in the Sierra Nevada: the Creek Fire was located directly west of Fresno and the SQF Complex composed of the Castle and Shotgun fires was located directly west of the EM27/SUN measurement site. This may be the reason that the peaks observed at the FTIR site are not seen in the Fresno AERONET data. Ahangar et al. (2022) determined that the SJV air quality was mainly impacted during the Sept. 8 – 15 period with Creek and SQF Complex fires responsible for the majority of the smoke within SJV. Although the Creek fire began on Sept. 5, the air quality began to deteriorate a few days after, possibly due to the westerly downslope winds that pushed the smoke east of the Sierra Nevada at the beginning of the fire (Cho et al., 2022). Low AOD from AERONET was observed prior to Sept. 8 with values of 0.50 ± 0.28, illustrating the air quality was cleaner and deteriorated after the activity from the Creek and SQF Complex fires increased (Ahangar et al., 2022).

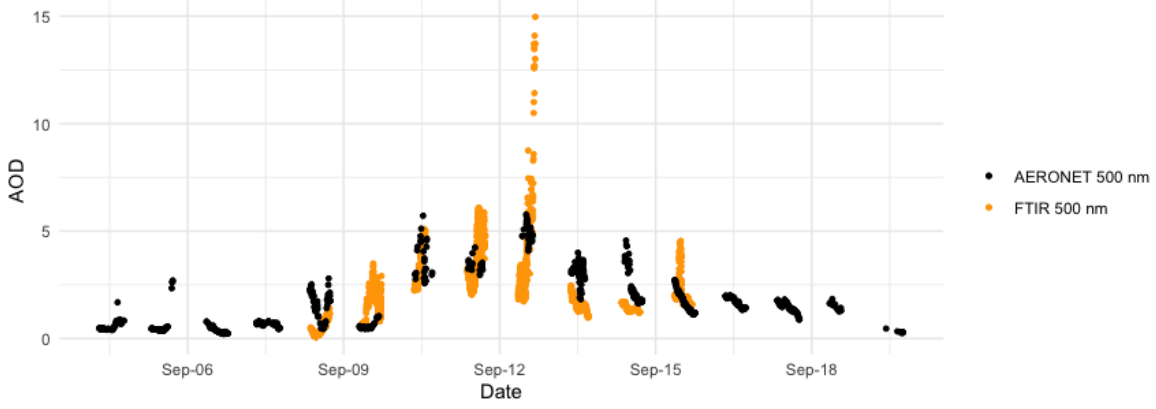

Figure 4. FTIR AOD and AERONET AOD at 500 nm. The FTIR AOD at this wavelength was calculated using the Ångström exponent relationship.

We find a strong correlation ($R^2 > 0.94$) between the EM27/SUN measured X_{CO} and AOD at 500 nm on most days with slopes ranging from 28.4 to 83.7 ppb CO/AOD (Figure 5). Several studies have shown strong correlation between CO and AOD at 500 and 550 nm from fire events and downwind of polluted sources (Lobert, 2002; Paton-Walsh et al., 2005; McMillan et al., 2008; Kampe and Sokolik, 2007). McMillan et al. (2008) found values for linear regression fits ranging from 44 to 74 from AIRS CO and MODIS AOD observations of fire plumes. Most of our slopes fall within this range and the lower slopes (Sept. 10 and 11) follow a similar linear trend (black line in Figure 5) as observed by McMillan et al. (2008) over a clean region during Alaskan/Canadian fires. The intercepts of the fitted lines reflect different local backgrounds of CO with

https://doi.org/10.5194/acp-2022-671
Preprint. Discussion started: 14 October 2022

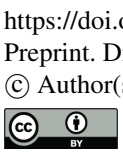

Atmospheric Chemistry and Physics Discussions

Sept. 12 having the largest background of 139 ppb. We find that the AOD on Sept. 12 reached values above 15 indicating extremely high aerosol loading from the smoke plume event transported from the SQF Complex in the Sierra Nevada.

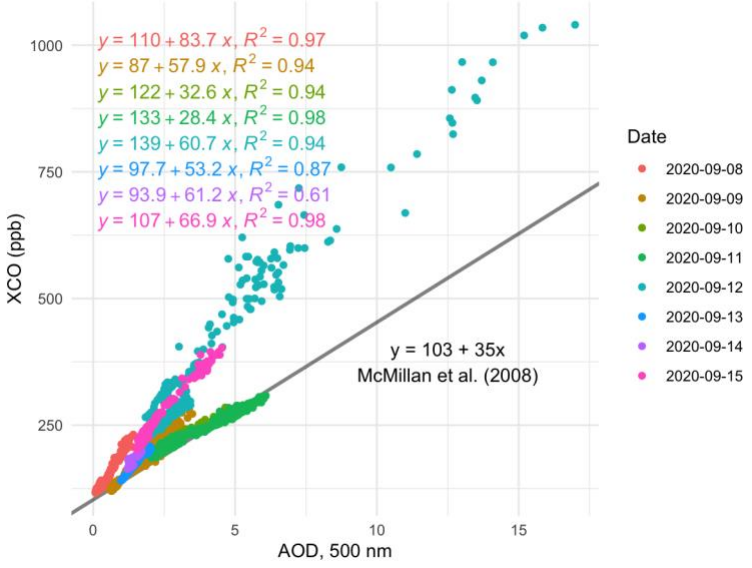

Figure 5. Scatterplot correlations of X_{CO} and AOD at 500 nm from the FTIR for each day of the first week Sept. 8 -12. Low smoke days fall along the black line, derived from previous remotely sensed X_{CO}/AOD relationships. The teal line corresponds to Sept. 12, the day of highest fire influence in our record.

3.4 Emissions factors and Modified Combustion Efficiency

The average MCE for the smoke plume on Sept. 12 was 0.89 ± 0.21, meaning that observations of the smoke plume consisted of a mixture of flaming and smoldering combustion phases (Figure 6). During the flaming phase of a fire, CO_2 is produced, and convection is created by high flame temperatures and produces lofting of smoke. High altitude smoke can be transported large distances, corroborated by observations of ash falling from the sky at the measurement site ~60 km away from the fire and clearly observable by satellite imagery (Figure 1b). In contrast to the flaming phase, smoldering fires burn at lower intensity, and incomplete combustion side products like CO, CH_4, and organic carbon aerosol are produced. We observed a steady MCE as X_{CO}, X_{CH4}, and AOD increased, indicating influence of smoldering combustion (Figure 6, a-e). The MCE calculated from total column observations is averaged over the entire vertical plume as it was being transported over the measurement site. The advantage of a plume integrated MCE is that vegetation is burnt differently throughout the fire and the atmospheric column observations can represent the fire as a whole by integrating the smoke plume heterogeneity in the vertical atmospheric column.

Emission ratios of CO and CH_4 on Sept. 12 were calculated with respect to CO_2. $ER_{CO/CO2}$ was 0.116 and the $ER_{CH4/CO2}$ was 0.0073 (Figure 6, f-h), resulting in an EF_{CO2} of 1632.9 ± 163.3 g CO_2 per kg biomass combusted, EF_{CO} of 120.5 ± 12.2 g CO per kg biomass combusted, and a EF_{CH4} of 4.3 ± 0.8 g CH_4 per kg biomass combusted. We compared findings from our

https://doi.org/10.5194/acp-2022-671
Preprint. Discussion started: 14 October 2022

Atmospheric Chemistry and Physics Discussions

gas measurements to literature values in temperate coniferous forest studies from the Sierra Nevada and other locations in North America summarized in Table 1 and Figure 7. All the studies listed in Table 1 except for this study were based on aircraft measurements. Most recently, Prichard et al. (2022) compiled emission factors for North American conifer forests and found a fire average for EF_{CO2} of 1629.54 ± 63.43, EF_{CO} of 104.01 ± 34.93, and EF_{CH4} of 5.05 ± 2.41. Burling et al. (2011) measured the Turtle Fire in the Sierra Nevada, and we find that our MCE overlaps within error with theirs. Finally, CH_4 emissions reported for more smoldering fires that were characterized by direct O_2/CO measurements for 1999 Big Bar fire (Lueker et al., 2001). Our atmospheric column-based EF fall within the ranges of previous literature, highlighting the ability of the EM27/SUN solar spectrometer observations to be used for deriving important variables for fire research.

Table 1. Summary of past airborne studies modified combustion efficiency (MCE) and emission factors (EF, g kg^{-1}) relative to CO_2 for temperate coniferous forests in North America and Sierra Nevada.

Studies	**MCE**	**EF CO_2**	**EF CO**	**EF CH_4**
North America				
Radke et al., 1991* – Conifer Forest	0.919	1641	93	3.03
Yokelson et al., 1999* – Southeastern US Pine Forest understory	0.926	1677	86	-
Yokelson et al., 2011 – Mexico Pine-oak	0.908	1603	103	3.66
Burling et al., 2011* –Average conifer forests understory burns	0.936 ± 0.024	1668 ± 72	72 ± 26	3.0 ± 2.4
Urbanski et al., 2013 – Rocky Mts conifer forest fires	0.85 – 0.92	1527 – 1681	89.3 – 173	4.4 – 12.1
Liu et al., 2017 – Study average	0.912	1454 ± 78	89.3 ± 28.5	4.9 ± 1.5
Sierra Nevada				
Burling et al., 2011				
Turtle Fire* (10-Nov-2009)	0.913	1599	97	5.51
Shaver Fire* (10-Nov-2009)	0.885	1523	126	7.94
Yates et al., 2016				
Rim fire (26-Aug-13)	0.94	1675 ± 285	92.5 ± 16	4.8 ± 0.8
Rim fire (29-Aug-13)	0.94	1711 ± 292	69.5 ± 12	4.7 ± 0.8
Rim fire (10-Sept 13)	0.88	1595 ± 272	138.4 ± 24	7.5 ± 1.3
Liu et al., 2017				
Rim fire (26-Aug-13)	0.923	1478 ± 11	78.7 ± 4	4.43 ± 0.25
This study: SQF Complex fire+ (12-Sept 22)	**0.89 ± 0.21**	**1632.9 ± 163.3**	**120.5 ± 12.2**	**4.3 ± 0.8**

*Prescribed burns
+ Measurement uncertainties were calculated by propagating the error from the linear regression standard error, C_T, and 10% error from $M_{Biomass}$.

https://doi.org/10.5194/acp-2022-671
Preprint. Discussion started: 14 October 2022

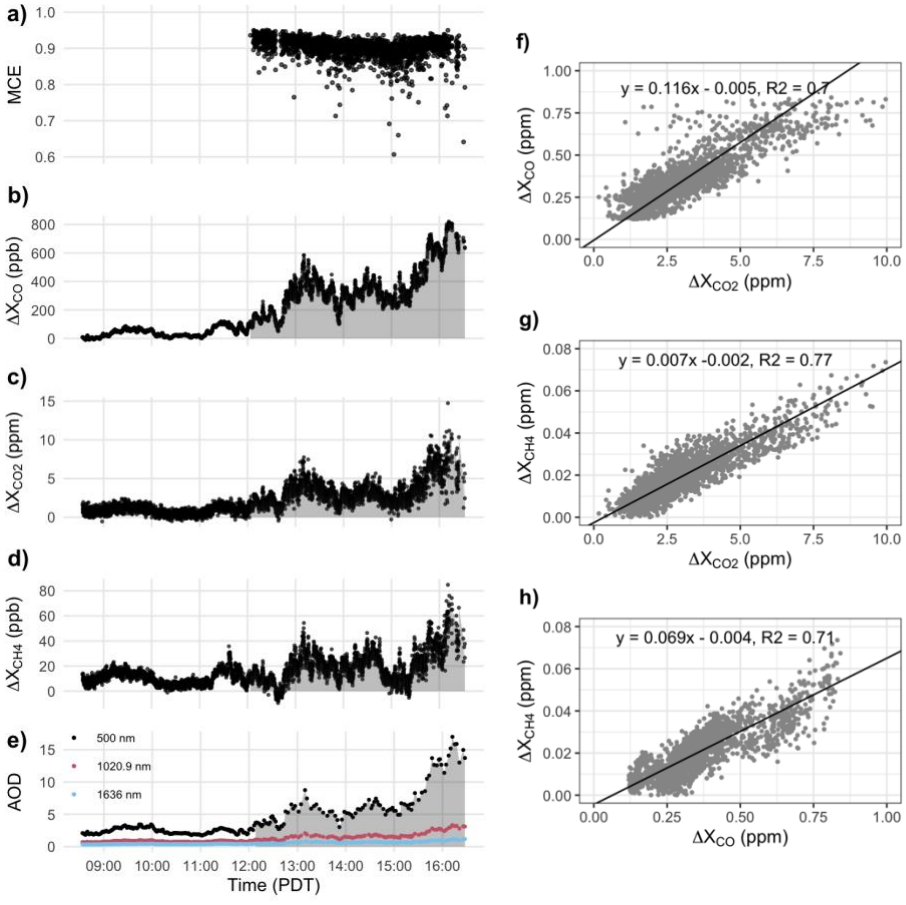

Figure 6. Timeseries of September 12, 2020 of a) MCE and b-e) ΔX_{CO}, ΔX_{CO2}, ΔX_{CH4}, and AOD with shaded grey area representing the SQF Complex fire plume. f-g) Type II linear regression plots of ΔCO and ΔCH_4 against ΔCO_2 and h) ΔCH_4 against ΔCO to calculate the slope that represents the ER.

https://doi.org/10.5194/acp-2022-671
Preprint. Discussion started: 14 October 2022

Atmospheric Chemistry and Physics Discussions

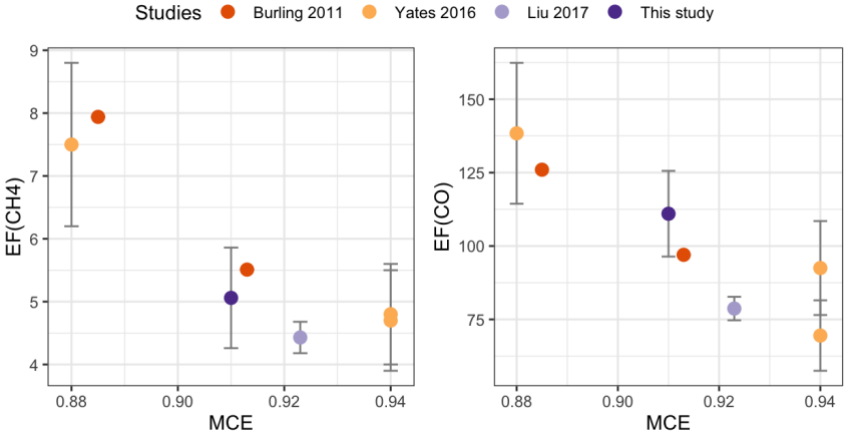

Figure 7. Emission factors (g kg^{-1}) as a function of MCE for temperate coniferous forests in Sierra Nevada wildfires.

3.5 Enhancement ratios of SJV greenhouse sources

The EM27/SUN's location enabled us to sample transient fire plumes from local and state wildfires, but was also located near a large cluster of dairy farms, which are a large regional source of CH_4 emissions (Heerah et al., 2021; Marklein et al., 2021). Dairy farms are known to emit significant amounts of CH_4 from the animal's enteric fermentation and on-farm manure management. Because fires also emit CH_4, we explored whether dairy and fire sources in this region can be disentangled using ratios of the different species measured by the EM27/SUN. Furthermore, our measured X_{CH4} enhancement ratios relative to X_{CO2} enable us to investigate the contribution of state wildfires to CH_4 emissions in 2020. To constrain the observed enhancements, we compared the enhancement ratios of $\Delta X_{CH4}/\Delta X_{CO2}$ from September – October 2020 to enhancement ratios collected in September 2018 and 2019 in the same local area that characterize non-fire years. September 2018 and 2019 measurements are further described in the supplemental information. We focused on observation days with statistically significant correlations (n = 26 days) between CH_4 and CO_2 enhancements ($R^2 > 0.5$ and $p < 0.05$) to characterize enhancement ratios of the SJV non-fire years.

Figure 8 shows the $\Delta X_{CH4}/\Delta X_{CO2}$ enhancement ratios from September 2018, September 2019, and September – October 2020 measurements. We observe a clear influence of dairy farms with larger $\Delta X_{CH4}/\Delta X_{CO2}$ enhancement ratios of 38.4 ± 21.7 and 30.5 ± 5.0 (ppb/ppm), respectively for September 2018 and 2019, exceeding $\Delta X_{CH4}/\Delta X_{CO2}$ wildfire smoke periods. During our 2020 observations, $\Delta X_{CH4}/\Delta X_{CO2}$ reflecting dairy farm influence were found on some days in addition to less steep slopes from smoke influence. This is expected as elevated X_{CO2} and lower X_{CH4} are emitted from wildfires. The Sept. 12 smoke plume event is highlighted in the figure and has a smaller enhancement ratio of 7.3 (ppb/ppm) than dairy farms. Similar ratios of $\Delta X_{CH4}/\Delta X_{CO2}$ were found in Hanford, ~50 km west of our observation site, from an aircraft study ranging from 35.9 – 44.4 (ppb/ppm) during a winter campaign (Herrera et al., 2021). Other column-based studies have determined the X_{CH4}/X_{CO2} for urban sources in the Los Angeles City finding ratios for X_{CH4}/X_{CO2} ranging from 6.65 to 9.96 (ppb/ppm) in 2015 (Chen et al., 2016). Wunch et al., 2009 calculated X_{CH4}/X_{CO2} ratio of 11 ± 2 and showed that urban fossil fuel and wildfire X_{CH4}/X_{CO2} ratios

https://doi.org/10.5194/acp-2022-671
Preprint. Discussion started: 14 October 2022


Atmospheric Chemistry and Physics Discussions

are very similar due to incomplete combustion and ratios are not distinct enough to separate (Wunch et al., 2009). In the vicinity of the measurement site in the SJV, there is a strong influence of dairy farm agriculture and minimal urban emissions away from population centers, thus we are able to separate of X_{CH4}/X_{CO2} from dairy sources, from fire or possible urban emissions. The CH_4/CO_2 enhancement ratios observed in this area make it evident that dairy farms operations are the dominant source of CH_4 during fire and non-fire periods. Nevertheless, CH_4 enhancements during the strong smoke influence periods greatly exceeded CH_4 enhancements from local dairy sources. The immense scale of 2020 wildfires, summing to 28% of the states' CO_2 budget for the year (CO2 Inventory Scoping Plan, 2022), in addition our observations of elevated fire-derived CH_4, suggest that these fires had a significant effect on the state's CH_4 budget.

Given the importance of reducing CH_4 emissions for meeting California's climate goals, we calculate the amount of CH_4 released from the wildfires that burnt in the state in 2020 using estimated CO_2 emissions from the state's wildfire inventory along with emission ratios of CH_4/CO_2 from our study and the literature on fires in California. The California Air Resources Board (CARB) reported CO_2 emissions of 106.7 Tg of CO_2 was emitted from 2020 wildfires, with individual CO_2 emission estimates from the top 20 wildfires. We use estimated CO_2 emissions from the top 20 wildfires to derive CH_4 emissions. The total emissions of CH_4 are calculated by multiplying the emission or enhancement ratio of wildfire smoke and molecular mass ratios:

$$E_{CH4} = \left(ER_{CH4} \times \frac{M_{CH4}}{M_{CO2}}\right) E_{CO2} \quad (8)$$

where E_{CH4} is the emissions of CH_4 in Gg/yr, ER_{CH4} with respect to CO_2 in mol/mol, M_{CH4} is the molar mass of CH_4 and M_{CO2} is the molar mass of CO_2, and E_{CO2} are the fire specific emissions in Gg/yr. ER from fires are dependent on vegetation type; fires in California fell into temperate forest, shrubland or grassland vegetation types (Xu et al., 2022). Based on the generic vegetation classification from the FINN model (https://www.acom.ucar.edu/Data/fire/), we classify the top 20 California wildfires of 2020 into the three types based on the dominant vegetation. The ER for the general vegetation was derived from EFs summarized in Xu et al., 2020 and for the Creek and SQF Complex fires we averaged the EFs summarized in Table 1 for the Sierra Nevada and derive an ER shown in Table E1, Appendix E. The top 20 wildfires represented 92% of CO_2 emissions released from wildfires in 2020 and emitted 213.7 ± 49.8 Gg CH_4. Figure 9 shows the estimated CH_4 emissions from the top 20 largest wildfires of 2020 compared to CARB's 2019 anthropogenic CH_4 inventory emissions, the most recent inventory year available (CH4 Inventory Scoping Plan, 2022).

https://doi.org/10.5194/acp-2022-671
Preprint. Discussion started: 14 October 2022

Atmospheric Chemistry and Physics Discussions

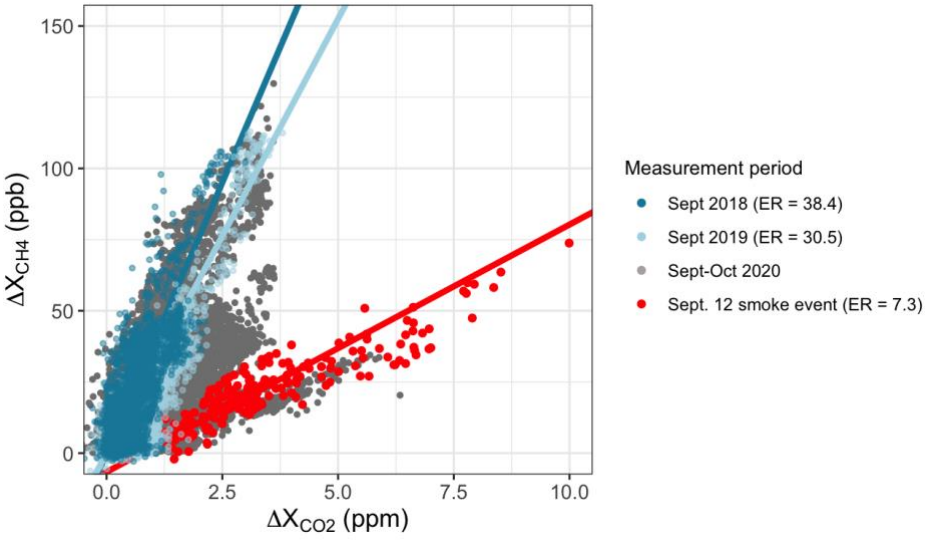

Figure 8. Correlation plots of ΔX_{CH4} vs ΔX_{CO2} for SJV measurements collected during non-fire years in Sept. 2018 (blue) and 2019 (light blue), and during fire period of Sept. – Oct. 2020 (gray). The Sept. 12 smoke event (red) highlighted with a linear fit through that day's data clearly shows a distinct $\Delta X_{CH4}/\Delta X_{CO2}$ relationship from other data.

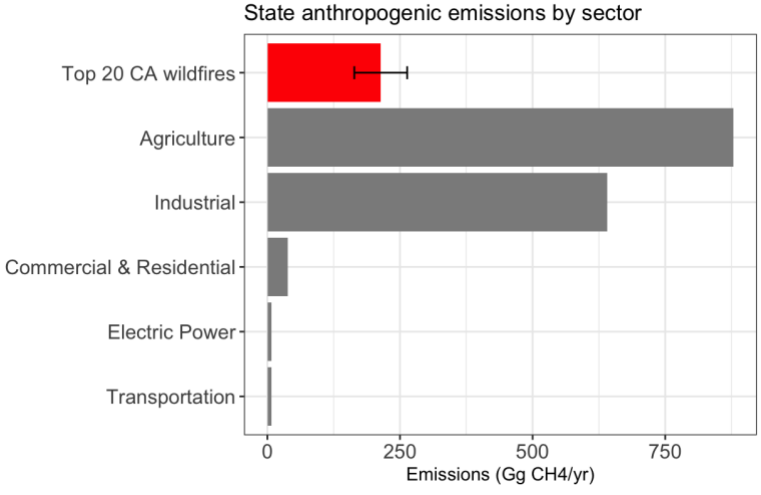

Figure 9. California CH_4 emissions from 2020 calculated for the top 20 wildfires compared to the state's anthropogenic CH_4 emissions from the 2019 inventory (CH4 Inventory Scoping Plan, 2022). The industrial sector also includes oil and gas emissions.

https://doi.org/10.5194/acp-2022-671
Preprint. Discussion started: 14 October 2022


Atmospheric Chemistry and Physics Discussions

4. Discussion

We made total column measurements of CO_2, CO, CH_4, and AOD with an EM27/SUN FTIR in the San Joaquin Valley (SJV), California during part of the wildfire season of 2020 from September to October. The emissions of the Creek and SQF Complex fires, two major wildfires burning in the Sierra Nevada, were sampled continuously in the SJV for over a month. We demonstrate that data from the EM27/SUN allows for calculating MCE and EFs in smoke plumes transported from wildfires, especially for high altitude smoke, adding important new estimates for fires in this region. For the Sierra Nevada, only three field-based studies have estimated emission factors in this area despite the increase in wildfires over burns the previous decade (Burling et al., 2011; Yates et al., 2016; Liu et al., 2017). Our emission factor estimates from the September 12 event for CO (120.5 ± 12.2 g kg^{-1} dry biomass burned) and CH_4 (4.3 ± 0.8 g kg^{-1} dry biomass burned) are within the range of those reported from the Sierra Nevada conifer forests (Burling et al., 2011; Yates et al., 2016; Liu et al., 2017). Our atmospheric column-based estimates contribute to the limited number of EF for temperate forests and are particularly important given the scale of the fires that occurred in 2020 in California.

Empirically quantified EFs in temperate conifer forests are limited in number and many of the measurements in these regions are from prescribed burning for land management (Burling et al., 2011; Akagi et al., 2011; Urbanski, 2013). Because prescribed burns typically occur during favorable atmospheric conditions, specified fuel, and during non-wildfire seasons, it is possible that prescribed burn EFs may not represent wildfire EFs that burn under different conditions favorable to wildfires (Urbanski, 2013). There is a need for biome-specific EFs to quantify the amount of trace gas or aerosol emitted per kilogram of biomass burned, and these EFs are essential model inputs for estimating total greenhouse gas and aerosol emissions of fires.

Field measurements have also been limited in measuring a smaller fraction of the smoke plume. Airborne measurements are the most common method to estimate EFs from wildfires and involve aircraft equipped with fast response gas analyzers sampling through smoke plumes (e.g. Yokelson et al., 1999; Yates et al., 2016; Iraci et al., 2022). Although highly effective for large and remote wildfires, this method can be costly and logistically complex, limiting the number of fires sampled during a campaign period (Ross et al., 2013). *In situ* stations downwind of fires are able to provide measurements when aircraft are unable to fly but they oversample in smoldering conditions where the fire burns less vigorously and emissions are released closer to the ground. Aircraft measurements tend to sample lofted fire samples in the flaming phase, resulting in different emissions than a fire *in situ* measurements (Paton-Walsh et al., 2005). Although much has been learned from these methods, an average sample of the fire plumes is difficult to obtain due to variability in emissions from the fire burning at different stages (Paton-Walsh et al., 2005). Open-path FTIR measurements have allowed for "whole-fire" emission factors (Smith et al., 2014). Total-column measurements can provide a plume-integrated EF and MCE; however, calculating EFs with respect to CO_2 in the vertical column has been challenging due to high atmospheric background (Kille et al., 2022; Paton-Walsh et al., 2005; Lutsch et al., 2020, 2016; Viatte et al., 2014, 2015). Portable solar viewing instruments like the EM27/SUN have the advantage of remotely sampling total columns closer to the source and capturing a vertical integration of transported smoke plumes, contributing to the limited number of EFs across biomes and understanding impact on regional smoke influence background.

https://doi.org/10.5194/acp-2022-671
Preprint. Discussion started: 14 October 2022


Atmospheric Chemistry and Physics Discussions

Simultaneous measurements of ground-based total columns and satellites allow for a spatial and temporal understanding of the fire events. The X_{CO} enhancement from the 2020 wildfires in the Sierra Nevada was also observed from space and smoke plumes up to ten times higher than the local background are visible in the TROPOMI soundings on the Sept. 12. smoke event. Pairing stationary ground-based column observations with satellites can help in understanding regional wildfires at a greater spatial and temporal scale. Although TROPOMI has daily global coverage with great resolution, daily snapshots are often not enough to understand the behavior of a fire. Conversely, stationary ground-based instruments are limited to observing a point in space. As an instrument with capability of measuring atmospheric columns, the EM27/SUN can help close the gap in the temporal scale of satellite observations. The EM27/SUN measured continuously in the daytime filling in the temporal gaps from the satellite TROPOMI's single overpass observations. A sensitivity study showed that a smaller radius of 5 or 15 km from TROPOMI observations paired with 30-minute averaging around the overpass time gave better statistical agreement during wildfire events. This strong correlation of X_{CO} between TROPOMI and the EM27/SUN has been observed before in urban sites (Sagar et al., 2022; Alberti et al., 2022b) and in rural Alaska (Jacobs, 2021). Jacobs (2021) found that wildfire influences in X_{CO} resulted in high observational variance in EM27/SUN observations and they suggest that this may be due to spatial and temporal variability in the smoke plume measured by TROPOMI and the EM27/SUN. The 9.7% overestimation from TROPOMI found in this study may also be due to averaging of the smoke plume's heterogeneity within each TROPOMI comparison point. Alternatively, Rowe et al. (2022) found that multiple scattering on aerosols may be responsible for 5-10% increased X_{CO} observations from TROPOMI in thick smoke plumes.

The air quality index in the SJV was at an all-time high in the hazardous range for weeks during the 2020 wildfire season (Morris III and Dennis, 2020) and AOD at the AERONET site in Fresno increased by three to five times higher than yearly average from 2002-2019 (Cho et al., 2022). FTIR-derived AOD at 500 nm reached extreme highs during the Sept. 12 smoke plume event, and followed the same trend on other days as the trace gas enhancements. The slopes during low smoke and high smoke days were consistent with previous satellite observations by McMillan et al. (2008). Previously, simultaneous measurements of aerosols and trace gases from the same instrument has been limited due to the aerosol burden interfering with retrieval of trace gases. For example, the majority of the TROPOMI X_{CH4} product was flagged out completely near the observational site during the Sept 7 – 15 period, and hence was not included in this analysis. The EM27/SUN demonstrated the potential to elucidate trace gas and aerosol relationships even during thick aerosol periods. Similarly, future studies may use simultaneous measurements from TROPOMI X_{CO} product and AOD to study regional impacts from wildfires (Chen et al., 2021). Scattered diffuse light during high aerosol loading from biomass burning may decrease the reliability of the AOD observations, thus further verification of the FTIR-derived AOD during high aerosol loading is required. Since the nearest AERONET station was relatively far away from our EM27/SUN site, we cannot do a true side-by-side comparison. However, the FTIR derived AOD showed the same baseline pattern as the AERONET site in Fresno, demonstrating the ability of the EM27 to simultaneously measure AOD and trace gases through a thick plume of smoke which can elucidate mechanisms within smoke plumes.

https://doi.org/10.5194/acp-2022-671
Preprint. Discussion started: 14 October 2022


Atmospheric Chemistry and Physics Discussions

As fires become more frequent with climate change, monitoring trace gases and particulates may become especially challenging in mixed source areas like the San Joaquin Valley where concentrations can become amplified by stagnant conditions in the SJV. Moreover, the fire-added CH_4 may hamper evaluation of greenhouse gas emission reduction initiatives at the state and at the global scale by adding unaccounted for CH_4 to the atmosphere. Using CARB's 2020 wildfire emission estimate for CO_2, we calculated the CH_4 contribution from the top 20 largest fires to be 213.7 ± 49.8 Gg CH_4, respectively. These wildfires alone emitted 13.6% of the total state CH_4 emissions, more than the transportation, electric power, and commercial and residential sectors. While estimated CH_4 emissions from wildfires are smaller in magnitude than inventoried emissions from agriculture and industrial sources, this source should be considered in the state's inventory given its magnitude and large impacts on the atmospheric CH_4 during wildfire periods. Additionally, wildfire emitted CH_4 may be an important and unaccounted positive feedback to climate change given the effect of increasing temperatures on fire severity.

5. Conclusions

Over the past 50 years, approximately three quarters of the area burned by wildfires in California's has been in North Coast and Sierra Nevada (Williams et al., 2019), highlighting the importance of studying emission factors from fires in these systems. However, there are surprisingly few observations of emission factors from these fires despite their importance to California's greenhouse gas budgets and air quality. The ground-based EM27/SUN is a useful instrument for understanding emissions of trace gases and aerosols from wildfires at a regional scales. The portable nature of the EM27/SUN allows for deployment downwind of fires for calculating important variables like EF and MCE. Having alternate techniques to calculate emission factors that are not costly or complex to deploy adds to the small number of emissions required to accurately calculate emissions and construct wildfire inventories. Several studies have demonstrated the utility in FTIR-derived EF for studying whole fire emissions from open path instruments (Paton-Walsh et al., 2014) and vertically integrated measurements (Viatte et al., 2013). Our total column MCE and EF with respect to CO_2 are the first to be reported from ground-based FTIR measurements in California.

Wildfire smoke produced overcast skies throughout the Western U.S. during this period, with smoke plumes transported long distances. The EM27 measures a vertically integrated regional signal but is limited spatially compared to observations from satellites. Here we show that a combination of the two can elucidate spatiotemporal variability of wildfire emissions. We find strong agreement between the EM27 and TROPOMI, but TROPOMI overestimates observations by 9.7%. This is consistent with previous studies of EM27 XCO in rural Alaska (Jacobs, 2021) and Idaho wildfires (Rowe et al., 2022). Additionally, our solar spectral measurements were used to derive AOD. We compared to a nearby AERONET site and found AOD values at 1020.9 and 1636 nm that were consistent with AERONET observations. The Ångström exponent was used to calculate FTIR AOD at 500 nm to compare AOD to CO ratios with previous studies. AOD at 500 nm reached extreme levels of up to 15 during the smoke plume event. Good agreements were found of AOD to CO ratios with those observed in McMillian et al., 2008 from MODIS AOD and AIRS CO.

https://doi.org/10.5194/acp-2022-671
Preprint. Discussion started: 14 October 2022


Atmospheric Chemistry and Physics Discussions

Finally, we find that a significant amount of CH_4 was emitted from the top 20 largest wildfires of 2020 in California. Given the importance of CH_4 emissions reduction for the state, our study suggests wildfires are an important source of CH_4 for California and may delay meeting the state's ambitious goals of reducing emissions. Atmospheric monitoring of CH_4 should account for wildfire periods, as they can significantly affect measured enhancements. Overall, our analysis demonstrates a novel application of the EM27/SUN solar spectrometers and will contribute to the development of techniques for analyzing remotely sensed greenhouse gas measurements from wildfires.

https://doi.org/10.5194/acp-2022-671
Preprint. Discussion started: 14 October 2022

Atmospheric Chemistry and Physics Discussions

Appendix A: EM27/SUN Correction Factors

The EM27/SUN was co-located with the CIT TCCON for 2-3 days before (Sept. 2 and 3, 2020) and after (Oct. 30, 31 and Nov. 31, 2020) the field measurements. A summary of the correction factors is shown in Table A1. An averaging kernel correction has been applied to the EM27/SUN observations prior to comparison following Hedelius et al. (2016). Due to a camera misalignment on Sept. 2 and 3, X_{CO} correction factors for those dates are not reported.

Table A1. Summary of correction factors from co-located EM27 measurements with TCCON at Caltech.

X_{gas}	Sept 2 & 3	Oct 30, 31 & Nov 1
X_{CH4}	0.9986 (0.0002)	0.9976 (0.0001)
X_{CO2}	1.0042 (0.0001)	1.0036 (0.0001)
X_{CO}	-	0.9737 (0.0028)
X_{H2O}	1.0044 (0.0005)	1.0101 (0.0005)

Appendix B: Aerosol Optical Depth

FTIR derived AOD was calculated by following the Langley exponential method where an absolute calibration, ln(Vo), is required.

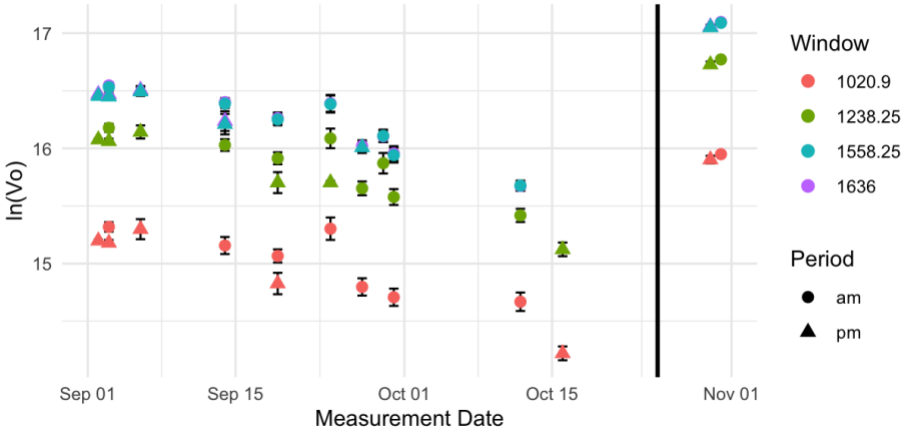

Figure B1. Absolute calibration for Langley exponential analysis of the EM27/SUN solar spectra over time from September to November 2020. Mirrors became significantly dirtier and dustier over the course of the measurement period. The ln(Vo) increased considerably after instrument mirrors were cleaned after the field campaign ended (black line).

https://doi.org/10.5194/acp-2022-671
Preprint. Discussion started: 14 October 2022

Atmospheric Chemistry and Physics Discussions

Table B1. Mean values of ln(Vo) from September 14, 19, and 24, 2020 used for deriving AOD.

Window	Mean ln(Vo)	sd	n
1020.9	15.17	0.11	3
1238.25	16.01	0.09	3
1558.25	16.34	0.08	3
1636	16.35	0.08	3

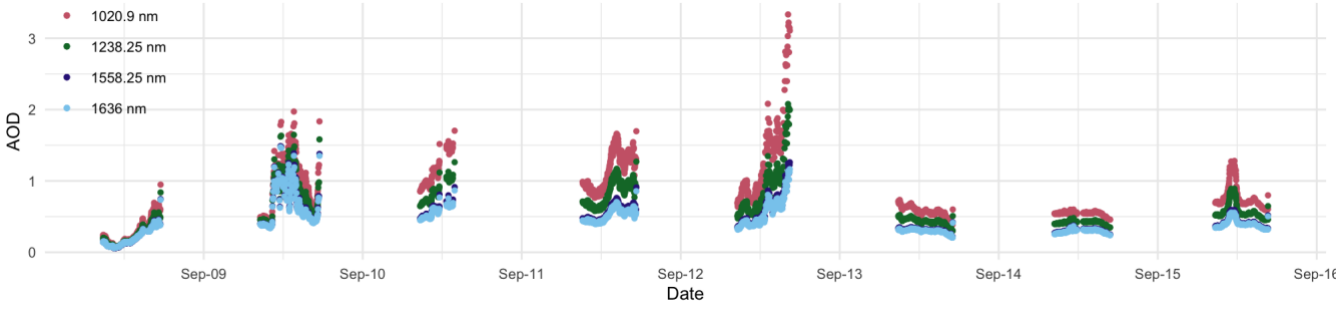

Figure B2. Timeseries of AOD for the four micro windows from September 8 to September 15, 2020.

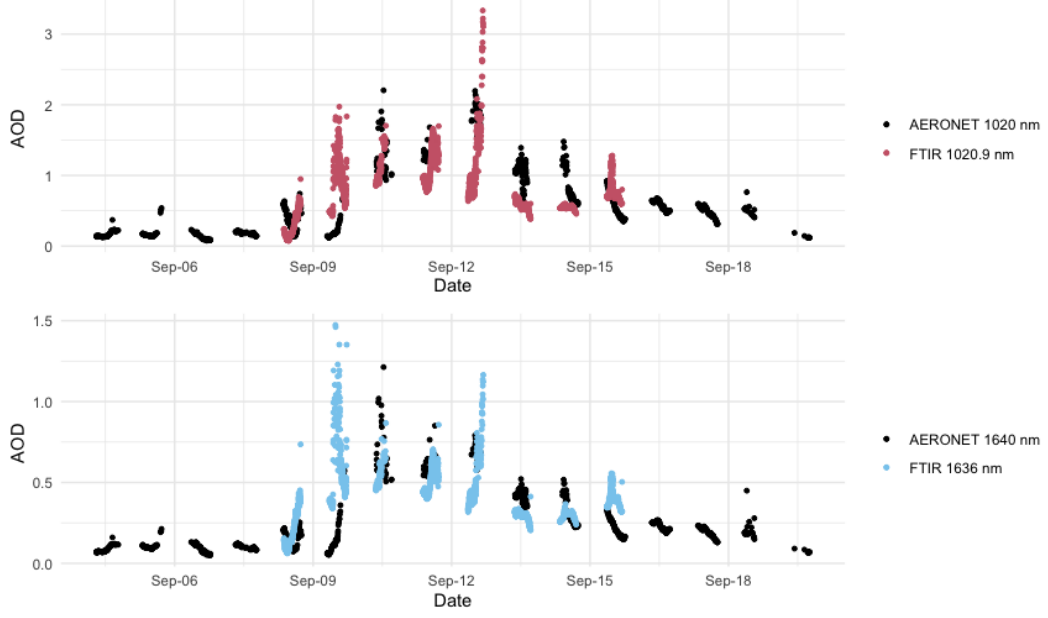

Figure B3. Timeseries of AOD from FTIR for the 1020.9 (red) and 1636 (blue) nm windows and AERONET (black) located in Fresno, CA ~90 km north of measurement site.

https://doi.org/10.5194/acp-2022-671
Preprint. Discussion started: 14 October 2022

Atmospheric Chemistry and Physics Discussions

Appendix C: EM27/SUN Sensitivity

595 The EM27/SUN has different instrument sensitivities defined by the averaging kernels (AK) for each species measured shown below in Figure C1. The difference in sensitivity for the trace gases may introduce a bias in calculated ERs and MCE. Most of the difference is expected to be at the height of the plume where the smoke is concentrated at 4.1 km (~600 hPa). Following the methods of Hedelius et al. (2018), we divide the enhancements of ΔX_{CO2} and ΔX_{CO} by the averaging kernel at that smoke plume height:

600

$$MCE_{AK\ corrected}\ (SZA) = \frac{\Delta CO2/AK(SZA)_{CO2,600\ hPa}}{\Delta CO2/AK(SZA)_{CO2,600\ hPa} + \Delta CO/AK(SZA)_{CO,600\ hPa}} \quad \text{(Eq. C1)}$$

where $AK_{600\ hPa}$ is the averaging kernel sensitivity for CO or CO_2. The mean relative difference of the correction for the Sept. 12 plume event is -1.1%, thus not applying this correction would overestimate the MCE by 1.1%

605

Similarly for the ERs, we correct the enhancements prior to fitting the points with a linear regression for the Sept. 12 plume event:

$$ER_{X,AK\ corrected} = \frac{\Delta X/AK(SZA)_{X,600\ hPa}}{\Delta X_{CO2}/AK(SZA)_{X,600\ hPa}} \quad \text{(Eq. C2)}$$

610

Without applying this correction, E_{CH4} would be underestimated by 9.5% and E_{CO} by 14.2% due to the difference in sensitivity.

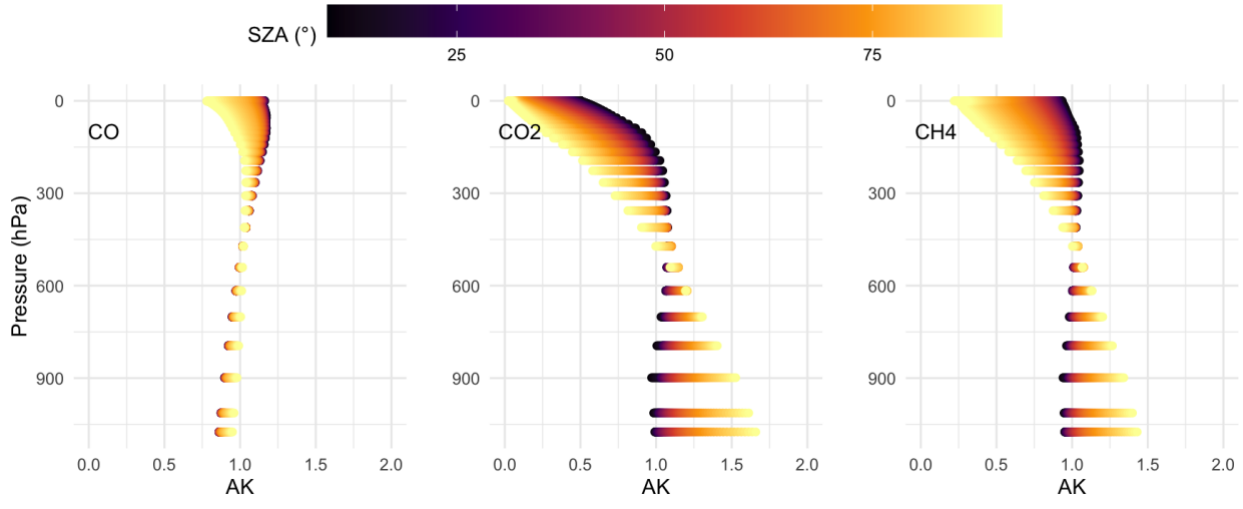

Figure C1. Averaging kernel (AK) of EM27/SUN of X_{CO} and X_{CO2} colored by solar zenith angle (SZA).

615

https://doi.org/10.5194/acp-2022-671
Preprint. Discussion started: 14 October 2022

Atmospheric Chemistry and Physics Discussions

Appendix D: TROPOMI and EM27/SUN

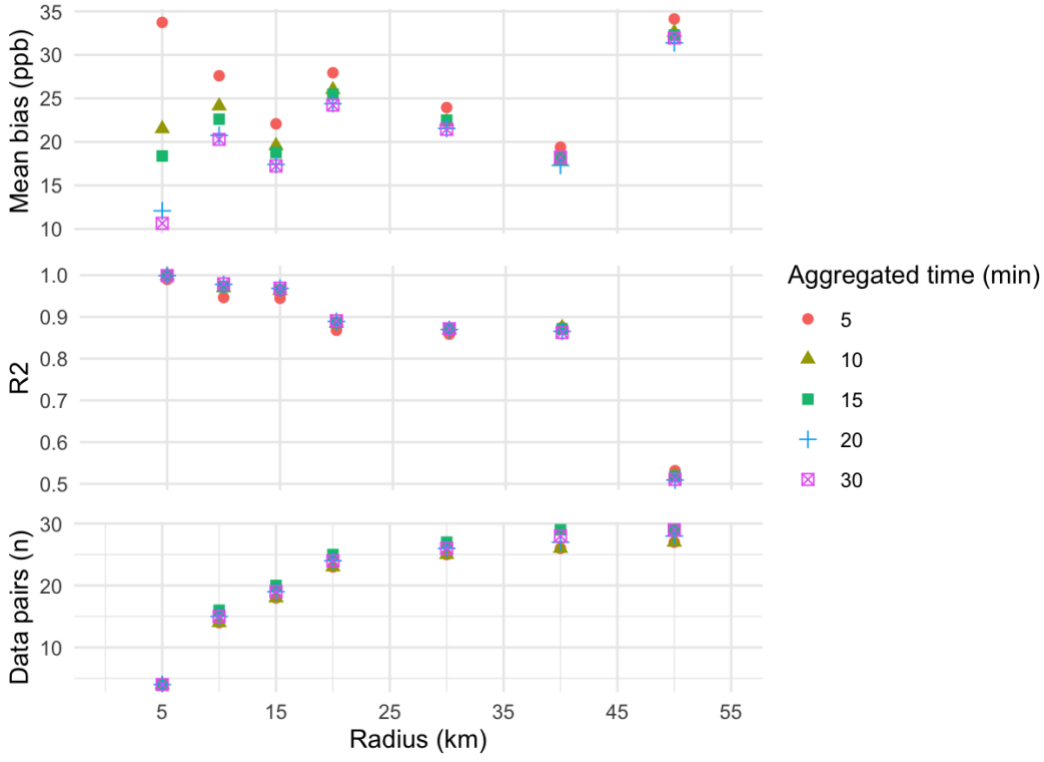

Figure D1. Results from sensitivity analysis with varying radius away from measurement site for selecting CO enhancements from TROPOMI pixels and varying aggregated times.

https://doi.org/10.5194/acp-2022-671
Preprint. Discussion started: 14 October 2022

Atmospheric Chemistry and Physics Discussions

Appendix E: Methane from wildfires

Table E1. Emissions of the top 20 of 2020 wildfires. Emission ratios for Sierra Nevada fires (Creek, Castle and North Complex) were derived from EFs compiled in this study. The rest of the ER are derived from literature (Prichard et al., 2020; Xu et al., 2022).

Fire Name	General Vegetation	Wildfire Area Burned (acres)	CO_2 (Tg)	ER_{CH4}	CH4 (Gg)
August Complex	Temperate evergreen	1,032,700	27.7	0.0055 ± 0.0044	55.4 ± 44.3
SCU Complex	Grasslands and savanna	396,399	4.6	0.0043 ± 0.0028	7.2 ± 4.7
Creek	**Temperate evergreen**	**379,882**	**13.8**	**0.0084 ± 0.0022**	**42.2 ± 11**
North Complex	Temperate evergreen	318,777	10.9	0.0084 ± 0.0022	33.3 ± 8.7
Hennessey	Shrublands	305,352	3.5	0.0033 ± 0.0021	4.2 ± 2.7
Castle	**Temperate evergreen**	**170,648**	**6.4**	**0.0084 ± 0.0022**	**19.5 ± 5.1**
Slater	Temperate evergreen	157,430	6.7	0.0055 ± 0.0044	13.4 ± 10.7
Red Salmon Complex	Temperate evergreen	143,836	4.6	0.0055 ± 0.0044	9.2 ± 7.4
Dolan	Shrublands	124,527	2.1	0.0033 ± 0.0021	2.5 ± 1.6
Bobcat	Shrublands	115,998	2.5	0.0033 ± 0.0021	3.0 ± 1.9
CZU Complex	Temperate evergreen	86,553	5.4	0.0055 ± 0.0044	10.8 ± 8.6
W-5 Cold Springs	Grasslands and savanna	84,817	0.7	0.0043 ± 0.0028	1.1 ± 0.7
Caldwell	Grasslands and savanna	81,224	0.4	0.0043 ± 0.0028	0.6 ± 0.4
Glass	Shrublands	67,484	1.9	0.0033 ± 0.0021	2.3 ± 1.4
Zogg	Shrublands	56,338	0.7	0.0033 ± 0.0021	0.8 ± 0.5
Wallbridge	Shrublands	55,209	4.1	0.0033 ± 0.0021	4.9 ± 3.1
River	Shrublands	50,214	0.9	0.0033 ± 0.0021	1.1 ± 0.7
Loyalton	Grasslands and savanna	46,721	0.7	0.0043 ± 0.0028	1.1 ± 0.7
Dome	Shrublands	44,211	0.1	0.0033 ± 0.0021	0.1 ± 0.1
Apple	Shrublands	33,209	0.8	0.0033 ± 0.0021	1.0 ± 0.6
Total					**213.7 ± 49.8**

https://doi.org/10.5194/acp-2022-671
Preprint. Discussion started: 14 October 2022

Atmospheric Chemistry and Physics Discussions

Data availability: TROPOMI data can be downloaded from https://s5phub.copernicus.eu (last access: 15 July 2022; ESA, 2022); TROPOMI aerosol layer height product can be downloaded from http://www.tropomi.eu/data-products/aerosol-layer-height (last access: 15 July 2022; ESA 2022); Satellite imagery captured by NOAA-20 VIIRS can be downloaded from https://worldview.earthdata.nasa.gov/ (last access: 15 July 2022; NASA 2022); AERONET data can be downloaded from http://aeronet.gsfc.nasa.gov/ (last access: 15 June 2022); Fire radiative power data can be downloaded from https://firms.modaps.eosdis.nasa.gov/ (last access: 15 June 2022), and PSL wind data can be downloaded from ftp://ftp1.psl.noaa.gov/psd2/data/realtime/Radar915/ (last access: 15 June 2022).

Author contribution: IFV and SH contributed to the manuscript via conceptualization and data curation. IFV and HAP contributed to the data collection. IFV, SH, and AGM contributed via formal analysis. The publication was written by IFV, and all authors reviewed the paper and contributed to the discussion of the paper. FMH and MD contributed to funding acquisition.

Competing interests: Some authors are members of the editorial board of ACP. The peer-review process was guided by an independent editor, and the authors have also no other competing interests to declare

Acknowledgements: We would also like to thank our funding source the University of California Office of the President Lab Fees Research Program (award LFR-18-548581) & National Science Foundation Graduate Research Fellowship Program. We thank Nicole Jacobs for providing code to apply the averaging kernel correction to EM27/SUN X_{CO} data. We thank Jacob Hedelius for providing code through EGI to read micro windows from EM27/SUN retrievals. The authors thank William Porter for the assistance and access to UCR-Aldo cluster.

https://doi.org/10.5194/acp-2022-671
Preprint. Discussion started: 14 October 2022

Atmospheric Chemistry and Physics Discussions

References

Aguilera, R., Corringham, T., Gershunov, A., and Benmarhnia, T.: Wildfire smoke impacts respiratory health more than fine particles from other sources: observational evidence from Southern California, Nat Commun, 12, 1493, https://doi.org/10.1038/s41467-021-21708-0, 2021.

Ahangar, F., Cobian-Iñiguez, J., and Cisneros, R.: Combining Regulatory Instruments and Low-Cost Sensors to Quantify the Effects of 2020 California Wildfires on PM2.5 in San Joaquin Valley, Fire, 5, 64, https://doi.org/10.3390/fire5030064, 2022.

Akagi, S. K., Yokelson, R. J., Wiedinmyer, C., Alvarado, M. J., Reid, J. S., Karl, T., Crounse, J. D., and Wennberg, P. O.: Emission factors for open and domestic biomass burning for use in atmospheric models, Atmos. Chem. Phys., 11, 4039–4072, https://doi.org/10.5194/acp-11-4039-2011, 2011.

Alberti, C., Hase, F., Frey, M., Dubravica, D., Blumenstock, T., Dehn, A., Castracane, P., Surawicz, G., Harig, R., Baier, B. C., Bès, C., Bi, J., Boesch, H., Butz, A., Cai, Z., Chen, J., Crowell, S. M., Deutscher, N. M., Ene, D., Franklin, J. E., García, O., Griffith, D., Grouiez, B., Grutter, M., Hamdouni, A., Houweling, S., Humpage, N., Jacobs, N., Jeong, S., Joly, L., Jones, N. B., Jouglet, D., Kivi, R., Kleinschek, R., Lopez, M., Medeiros, D. J., Morino, I., Mostafavipak, N., Müller, A., Ohyama, H., Palmer, P. I., Pathakoti, M., Pollard, D. F., Raffalski, U., Ramonet, M., Ramsay, R., Sha, M. K., Shiomi, K., Simpson, W., Stremme, W., Sun, Y., Tanimoto, H., Té, Y., Tsidu, G. M., Velazco, V. A., Vogel, F., Watanabe, M., Wei, C., Wunch, D., Yamasoe, M., Zhang, L., and Orphal, J.: Improved calibration procedures for the EM27/SUN spectrometers of the COllaborative Carbon Column Observing Network (COCCON), Atmos. Meas. Tech., 15, 2433–2463, https://doi.org/10.5194/amt-15-2433-2022, 2022a.

Alberti, C., Tu, Q., Hase, F., Makarova, M. V., Gribanov, K., Foka, S. C., Zakharov, V., Blumenstock, T., Buchwitz, M., Diekmann, C., Ertl, B., Frey, M. M., Imhasin, H. Kh., Ionov, D. V., Khosrawi, F., Osipov, S. I., Reuter, M., Schneider, M., and Warneke, T.: Investigation of spaceborne trace gas products over St Petersburg and Yekaterinburg, Russia, by using COllaborative Column Carbon Observing Network (COCCON) observations, Atmos. Meas. Tech., 15, 2199–2229, https://doi.org/10.5194/amt-15-2199-2022, 2022b.

Andreae, M. O.: Emission of trace gases and aerosols from biomass burning – an updated assessment, Atmos. Chem. Phys., 19, 8523–8546, https://doi.org/10.5194/acp-19-8523-2019, 2019.

Burling, I. R., Yokelson, R. J., Griffith, D. W. T., Johnson, T. J., Veres, P., Roberts, J. M., Warneke, C., Urbanski, S. P., Reardon, J., Weise, D. R., Hao, W. M., and de Gouw, J.: Laboratory measurements of trace gas emissions from biomass burning of fuel types from the southeastern and southwestern United States, Atmos. Chem. Phys., 10, 11115–11130, https://doi.org/10.5194/acp-10-11115-2010, 2010.

Burling, I. R., Yokelson, R. J., Akagi, S. K., Urbanski, S. P., Wold, C. E., Griffith, D. W. T., Johnson, T. J., Reardon, J., and Weise, D. R.: Airborne and ground-based measurements of the trace gases and particles emitted by prescribed fires in the United States, Atmos. Chem. Phys., 11, 12197–12216, https://doi.org/10.5194/acp-11-12197-2011, 2011.

CARB: An Inventory of Ecosystem Carbon in California's Natural & Working Lands, 2018.

CH4 Inventory Scoping Plan: https://ww3.arb.ca.gov/cc/inventory/data/tables/ghg_inventory_scopingplan_2000-19ch4.pdf, last access: 21 August 2022.

CO2 Inventory Scoping Plan: https://ww3.arb.ca.gov/cc/inventory/data/tables/ghg_inventory_scopingplan_2000-19co2.pdf, last access: 21 August 2022.

California Wildfire Emission Estimates: https://ww2.arb.ca.gov/wildfire-emissions, last access: 30 May 2021.

Chen, J., Viatte, C., Hedelius, J. K., Jones, T., Franklin, J. E., Parker, H., Gottlieb, E. W., Wennberg, P. O., Dubey, M. K., and Wofsy, S. C.: Differential column measurements using compact solar-tracking spectrometers, Atmos. Chem. Phys., 16, 8479–8498, https://doi.org/10.5194/acp-16-8479-2016, 2016.

Chen, X., Wang, J., Xu, X., Zhou, M., Zhang, H., Castro Garcia, L., Colarco, P. R., Janz, S. J., Yorks, J., McGill, M., Reid, J. S., de Graaf, M., and Kondragunta, S.: First retrieval of absorbing aerosol height over dark target using TROPOMI oxygen B band: Algorithm development and application for surface particulate matter estimates, Remote Sensing of Environment, 265, 112674, https://doi.org/10.1016/j.rse.2021.112674, 2021.

Cho, C., Kim, S.-W., Choi, W., and Kim, M.-H.: Significant light absorption of brown carbon during the 2020 California wildfires, Science of The Total Environment, 813, 152453, https://doi.org/10.1016/j.scitotenv.2021.152453, 2022.

De Mazière, M., Thompson, A. M., Kurylo, M. J., Wild, J. D., Bernhard, G., Blumenstock, T., Braathen, G. O., Hannigan, J. W., Lambert, J.-C., Leblanc, T., McGee, T. J., Nedoluha, G., Petropavlovskikh, I., Seckmeyer, G., Simon, P. C., Steinbrecht, W., and Strahan, S. E.: The Network for the Detection of Atmospheric Composition Change (NDACC): history, status and perspectives, Atmos. Chem. Phys., 18, 4935–4964, https://doi.org/10.5194/acp-18-4935-2018, 2018.

Dietrich, F., Chen, J., Voggenreiter, B., Aigner, P., Nachtigall, N., and Reger, B.: MUCCnet: Munich Urban Carbon Column network, Atmos. Meas. Tech., 14, 1111–1126, https://doi.org/10.5194/amt-14-1111-2021, 2021.

Frey, M., Sha, M. K., Hase, F., Kiel, M., Blumenstock, T., Harig, R., Surawicz, G., Deutscher, N. M., Shiomi, K., Franklin, J. E., Bösch, H., Chen, J., Grutter, M., Ohyama, H., Sun, Y., Butz, A., Mengistu Tsidu, G., Ene, D., Wunch, D., Cao, Z., Garcia, O., Ramonet, M., Vogel, F., and Orphal, J.: Building the COllaborative Carbon Column Observing Network (COCCON): long-term stability and ensemble performance of the EM27/SUN Fourier transform spectrometer, Atmos. Meas. Tech., 12, 1513–1530, https://doi.org/10.5194/amt-12-1513-2019, 2019.

Gutierrez, A. A., Hantson, S., Langenbrunner, B., Chen, B., Jin, Y., Goulden, M. L., and Randerson, J. T.: Wildfire response to changing daily temperature extremes in California's Sierra Nevada, Sci. Adv., 7, eabe6417, https://doi.org/10.1126/sciadv.abe6417, 2021.

Hase, F., Frey, M., Kiel, M., Blumenstock, T., Harig, R., Keens, A., and Orphal, J.: Addition of a channel for XCO observations to a portable FTIR spectrometer for greenhouse gas measurements, Atmos. Meas. Tech., 9, 2303–2313, https://doi.org/10.5194/amt-9-2303-2016, 2016.

Hedelius, J. K., Viatte, C., Wunch, D., Roehl, C. M., Toon, G. C., Chen, J., Jones, T., Wofsy, S. C., Franklin, J. E., Parker, H., Dubey, M. K., and Wennberg, P. O.: Assessment of errors and biases in retrievals of XCO2, XCH4, XCO, and XN2O from a 0.5 cm−1 resolution solar-viewing spectrometer, Atmos. Meas. Tech., 20, 2016.

Heerah, S., Frausto-Vicencio, I., Jeong, S., Marklein, A. R., Ding, Y., Meyer, A. G., Parker, H. A., Fischer, M. L., Franklin, J. E., Hopkins, F. M., and Dubey, M.: Dairy Methane Emissions in California's San Joaquin Valley Inferred With Ground-Based Remote Sensing Observations in the Summer and Winter, JGR Atmospheres, 126, https://doi.org/10.1029/2021JD034785, 2021.

Herrera, S. A., Diskin, G. S., Harward, C., Sachse, G., De Wekker, S. F. J., Yang, M., Choi, Y., Wisthaler, A., Mallia, D. V., and Pusede, S. E.: Wintertime Nitrous Oxide Emissions in the San Joaquin Valley of California Estimated from Aircraft Observations, Environ. Sci. Technol., 55, 4462–4473, https://doi.org/10.1021/acs.est.0c08418, 2021.

IPCC: Climate Change 2014: Mitigation of Climate Change. Working Group III Contribution to the Fifth Assessment Report of the Intergovernmental Panel on Climate Change, edited by: Edenhofer, O., Pichis-Madruga, R., Sokona, Y., Farahani, E.,

Kadner, S., Seyboth, A., Adler, A., Baum, I., Brunner, S., Eickmeier, P., Kriemann, B., Savolainen, J., Schlomer, S., von Stechow, C., and Zwickel, T., Cambridge University Press, New York, NY, 1435 pp., 2014.

Jacobs, N.: Vetting Model and Satellite-Based Estimates of Regional Scale Carbon Exchange at Northern High Latitudes Using Solar-Viewing Infrared Spectroscopy, ProQuest Dissertations Publishing, 2021.

Jain, P., Castellanos-Acuna, D., Coogan, S. C. P., Abatzoglou, J. T., and Flannigan, M. D.: Observed increases in extreme fire weather driven by atmospheric humidity and temperature, Nat. Clim. Chang., 12, 63–70, https://doi.org/10.1038/s41558-021-01224-1, 2022.

Kalnay, E., Kanamitsu, M., Kistler, R., Collins, W., Deaven, D., Gandin, L., Iredell, M., Saha, S., White, G., Woollen, J., Zhu, Y., Chelliah, M., Ebisuzaki, W., Higgins, W., Janowiak, J., Mo, K. C., Ropelewski, C., Wang, J., Leetmaa, A., Reynolds, R., Jenne, R., and Joseph, D.: The NCEP/NCAR 40-Year Reanalysis Project, Bulletin of the American Meteorological Society, 77, 437–472, https://doi.org/10.1175/1520-0477(1996)077<0437:TNYRP>2.0.CO;2, 1996.

Kampe, T. U. and Sokolik, I. N.: Remote sensing retrievals of fine mode aerosol optical depth and impacts on its correlation with CO from biomass burning, Geophys. Res. Lett., 34, L12806, https://doi.org/10.1029/2007GL029805, 2007.

Kille, N., Zarzana, K. J., Alvarez, J. R., Lee, C. F., Rowe, J. P., Howard, B., Campos, T., Hills, A., Hornbrook, R. S., Ortega, I., Permar, W., Ku, I. T., Lindaas, J., Pollack, I. B., Sullivan, A. P., Zhou, Y., Fredrickson, C. D., Palm, B. B., Peng, Q., Apel, E. C., Hu, L., Collett, J. L., Fischer, E. V., Flocke, F., Hannigan, J. W., Thornton, J., and Volkamer, R.: The CU Airborne Solar Occultation Flux Instrument: Performance Evaluation during BB-FLUX, ACS Earth and Space Chemistry, 15, 2022.

Li, M., Karu, E., Brenninkmeijer, C., Fischer, H., Lelieveld, J., and Williams, J.: Tropospheric OH and stratospheric OH and Cl concentrations determined from CH4, CH3Cl, and SF6 measurements, npj Clim Atmos Sci, 1, 1–7, https://doi.org/10.1038/s41612-018-0041-9, 2018.

Lindenmaier, R., Dubey, M. K., Henderson, B. G., Butterfield, Z. T., Herman, J. R., Rahn, T., and Lee, S.-H.: Multiscale observations of CO_2, $^{13}CO_2$, and pollutants at Four Corners for emission verification and attribution, Proc. Natl. Acad. Sci. U.S.A., 111, 8386–8391, https://doi.org/10.1073/pnas.1321883111, 2014.

Liu, X., Huey, L. G., Yokelson, R. J., Selimovic, V., Simpson, I. J., Müller, M., Jimenez, J. L., Campuzano-Jost, P., Beyersdorf, A. J., Blake, D. R., Butterfield, Z., Choi, Y., Crounse, J. D., Day, D. A., Diskin, G. S., Dubey, M. K., Fortner, E., Hanisco, T. F., Hu, W., King, L. E., Kleinman, L., Meinardi, S., Mikoviny, T., Onasch, T. B., Palm, B. B., Peischl, J., Pollack, I. B., Ryerson, T. B., Sachse, G. W., Sedlacek, A. J., Shilling, J. E., Springston, S., St. Clair, J. M., Tanner, D. J., Teng, A. P., Wennberg, P. O., Wisthaler, A., and Wolfe, G. M.: Airborne measurements of western U.S. wildfire emissions: Comparison with prescribed burning and air quality implications, JGR Atmospheres, 122, 6108–6129, https://doi.org/10.1002/2016JD026315, 2017.

Lobert, J. M.: Trace gases and air mass origin at Kaashidhoo, Indian Ocean, J. Geophys. Res., 107, 8013, https://doi.org/10.1029/2001JD000731, 2002.

Lueker, T. J., Keeling, R. F., and Dubey, M. K.: The oxygen to carbon dioxide ratios observed in emissions from a wildfire in northern California, Geophys. Res. Lett., 28, 2413–2416, https://doi.org/10.1029/2000GL011860, 2001.

Lutsch, E., Dammers, E., Conway, S., and Strong, K.: Long-range transport of NH_3, CO, HCN, and C_2H_6 from the 2014 Canadian Wildfires: CANADIAN WILDFIRE EMISSIONS OF NH_3, Geophys. Res. Lett., 43, 8286–8297, https://doi.org/10.1002/2016GL070114, 2016.

https://doi.org/10.5194/acp-2022-671
Preprint. Discussion started: 14 October 2022

Lutsch, E., Strong, K., Jones, D. B. A., Blumenstock, T., Conway, S., Fisher, J. A., Hannigan, J. W., Hase, F., Kasai, Y., Mahieu, E., Makarova, M., Morino, I., Nagahama, T., Notholt, J., Ortega, I., Palm, M., Poberovskii, A. V., Sussmann, R., and Warneke, T.: Detection and attribution of wildfire pollution in the Arctic and northern midlatitudes using a network of Fourier-transform infrared spectrometers and GEOS-Chem, Atmos. Chem. Phys., 20, 12813–12851, https://doi.org/10.5194/acp-20-12813-2020, 2020.

Makarova, M. V., Alberti, C., Ionov, D. V., Hase, F., Foka, S. C., Blumenstock, T., Warneke, T., Virolainen, Y. A., Kostsov, V. S., Frey, M., Poberovskii, A. V., Timofeyev, Y. M., Paramonova, N. N., Volkova, K. A., Zaitsev, N. A., Biryukov, E. Y., Osipov, S. I., Makarov, B. K., Polyakov, A. V., Ivakhov, V. M., Imhasin, H. Kh., and Mikhailov, E. F.: Emission Monitoring Mobile Experiment (EMME): an overview and first results of the St. Petersburg megacity campaign 2019, Atmos. Meas. Tech., 14, 1047–1073, https://doi.org/10.5194/amt-14-1047-2021, 2021.

Marklein, A. R., Meyer, D., Fischer, M. L., Jeong, S., Rafiq, T., Carr, M., and Hopkins, F. M.: Facility-scale inventory of dairy methane emissions in California: implications for mitigation, Earth Syst. Sci. Data, 13, 1151–1166, https://doi.org/10.5194/essd-13-1151-2021, 2021.

McKain, K., Down, A., Raciti, S. M., Budney, J., Hutyra, L. R., Floerchinger, C., Herndon, S. C., Nehrkorn, T., Zahniser, M. S., Jackson, R. B., Phillips, N., and Wofsy, S. C.: Methane emissions from natural gas infrastructure and use in the urban region of Boston, Massachusetts, Proc. Natl. Acad. Sci. U.S.A., 112, 1941–1946, https://doi.org/10.1073/pnas.1416261112, 2015.

McMillan, W. W., Warner, J. X., Comer, M. M., Maddy, E., Chu, A., Sparling, L., Eloranta, E., Hoff, R., Sachse, G., Barnet, C., Razenkov, I., and Wolf, W.: AIRS views transport from 12 to 22 July 2004 Alaskan/Canadian fires: Correlation of AIRS CO and MODIS AOD with forward trajectories and comparison of AIRS CO retrievals with DC-8 in situ measurements during INTEX-A/ICARTT, J. Geophys. Res., 113, D20301, https://doi.org/10.1029/2007JD009711, 2008.

Morris III, G. and Dennis, C.: 2020 Fire Siege, CALFIRE, 2020.

Navarro, K. M., Cisneros, R., and Balmes, J. R.: Air-Quality Impacts and Intake Fraction of PM2.5 during the 2013 Rim Megafire, Environ. Sci. Technol., 9, 2016.

Paton-Walsh, C., Jones, N. B., Wilson, S. R., Haverd, V., Meier, A., Griffith, D. W. T., and Rinsland, C. P.: Measurements of trace gas emissions from Australian forest fires and correlations with coincident measurements of aerosol optical depth, J. Geophys. Res., 110, D24305, https://doi.org/10.1029/2005JD006202, 2005.

Paton-Walsh, C., Smith, T. E. L., Young, E. L., Griffith, D. W. T., and Guérette, É.-A.: New emission factors for Australian vegetation fires measured using open-path Fourier transform infrared spectroscopy – Part 1: Methods and Australian temperate forest fires, Atmos. Chem. Phys., 14, 11313–11333, https://doi.org/10.5194/acp-14-11313-2014, 2014.

Porter, J. N., Miller, M., Pietras, C., and Motell, C.: Ship-Based Sun Photometer Measurements Using Microtops Sun Photometers, J. Atmos. Oceanic Technol., 18, 765–774, https://doi.org/10.1175/1520-0426(2001)018<0765:SBSPMU>2.0.CO;2, 2001.

Prichard, S. J., O'Neill, S. M., Eagle, P., Andreu, A. G., Drye, B., Dubowy, J., Urbanski, S., and Strand, T. M.: Wildland fire emission factors in North America: synthesis of existing data, measurement needs and management applications, Int. J. Wildland Fire, 29, 132, https://doi.org/10.1071/WF19066, 2020.

Ross, A. N., Wooster, M. J., Boesch, H., and Parker, R.: First satellite measurements of carbon dioxide and methane emission ratios in wildfire plumes: GOSAT MEASURE OF CO_2:CH_4 EMISSION RATIO, Geophys. Res. Lett., 40, 4098–4102, https://doi.org/10.1002/grl.50733, 2013.

Rowe, J. P., Zarzana, K. J., Kille, N., Borsdorff, T., Goudar, M., Lee, C. F., Koenig, T. K., Romero-Alvarez, J., Campos, T., Knote, C., Theys, N., Landgraf, J., and Volkamer, R.: Carbon Monoxide in Optically Thick Wildfire Smoke: Evaluating TROPOMI Using CU Airborne SOF Column Observations, ACS Earth Space Chem., 6, 1799–1812, https://doi.org/10.1021/acsearthspacechem.2c00048, 2022.

Sagar, V. K., Pathakoti, M., D.V., M., K.S., R., M.V.R., S. S., Hase, F., Dubravica, D., and Sha, M. K.: Ground-Based Remote Sensing of Total Columnar CO_2, CH_4, and CO Using EM27/SUN FTIR Spectrometer at a Suburban Location (Shadnagar) in India and Validation of Sentinel-5P/TROPOMI, IEEE Geosci. Remote Sensing Lett., 19, 1–5, https://doi.org/10.1109/LGRS.2022.3171216, 2022.

Schneising, O., Buchwitz, M., Reuter, M., Bovensmann, H., and Burrows, J. P.: Severe Californian wildfires in November 2018 observed from space: the carbon monoxide perspective, Atmos. Chem. Phys., 20, 3317–3332, https://doi.org/10.5194/acp-20-3317-2020, 2020.

Sha, M. K., Langerock, B., Blavier, J.-F. L., Blumenstock, T., Borsdorff, T., Buschmann, M., Dehn, A., De Mazière, M., Deutscher, N. M., Feist, D. G., García, O. E., Griffith, D. W. T., Grutter, M., Hannigan, J. W., Hase, F., Heikkinen, P., Hermans, C., Iraci, L. T., Jeseck, P., Jones, N., Kivi, R., Kumps, N., Landgraf, J., Lorente, A., Mahieu, E., Makarova, M. V., Mellqvist, J., Metzger, J.-M., Morino, I., Nagahama, T., Notholt, J., Ohyama, H., Ortega, I., Palm, M., Petri, C., Pollard, D. F., Rettinger, M., Robinson, J., Roche, S., Roehl, C. M., Röhling, A. N., Rousogenous, C., Schneider, M., Shiomi, K., Smale, D., Stremme, W., Strong, K., Sussmann, R., Té, Y., Uchino, O., Velazco, V. A., Vigouroux, C., Vrekoussis, M., Wang, P., Warneke, T., Wizenberg, T., Wunch, D., Yamanouchi, S., Yang, Y., and Zhou, M.: Validation of methane and carbon monoxide from Sentinel-5 Precursor using TCCON and NDACC-IRWG stations, Atmos. Meas. Tech., 14, 6249–6304, https://doi.org/10.5194/amt-14-6249-2021, 2021.

Smith, T. E. L., Paton-Walsh, C., Meyer, C. P., Cook, G. D., Maier, S. W., Russell-Smith, J., Wooster, M. J., and Yates, C. P.: New emission factors for Australian vegetation fires measured using open-path Fourier transform infrared spectroscopy – Part 2: Australian tropical savanna fires, Atmos. Chem. Phys., 14, 11335–11352, https://doi.org/10.5194/acp-14-11335-2014, 2014.

Sommers, W. T., Loehman, R. A., and Hardy, C. C.: Wildland fire emissions, carbon, and climate: Science overview and knowledge needs, Forest Ecology and Management, 317, 1–8, https://doi.org/10.1016/j.foreco.2013.12.014, 2014.

Stephensen, N. and Brigham, C.: Preliminary Estimates of Sequoia Mortality in the 2020 Castle Fire (U.S. National Park Service), 2021.

Toon, G., Blavier, J.-F., Washenfelder, R., Wunch, D., Keppel-Aleks, G., Wennberg, P., Connor, B., Sherlock, V., Griffith, D., Deutscher, N., and Notholt, J.: Total Column Carbon Observing Network (TCCON), in: Advances in Imaging, Fourier Transform Spectroscopy, Vancouver, JMA3, https://doi.org/10.1364/FTS.2009.JMA3, 2009.

UNEP: Spreading like Wildfire – The Rising Threat of Extraordinary Landscape Fires, United Nations Environment Programme, Nairobi, 2022.

Urbanski, S.: Wildland fire emissions, carbon, and climate: Emission factors, Forest Ecology and Management, 317, 51–60, https://doi.org/10.1016/j.foreco.2013.05.045, 2014.

Urbanski, S. P.: Combustion efficiency and emission factors for wildfire-season fires in mixed conifer forests of the northern Rocky Mountains, US, Atmos. Chem. Phys., 13, 7241–7262, https://doi.org/10.5194/acp-13-7241-2013, 2013.

Veefkind, J. P., Aben, I., McMullan, K., Förster, H., de Vries, J., Otter, G., Claas, J., Eskes, H. J., de Haan, J. F., Kleipool, Q., van Weele, M., Hasekamp, O., Hoogeveen, R., Landgraf, J., Snel, R., Tol, P., Ingmann, P., Voors, R., Kruizinga, B., Vink, R., Visser, H., and Levelt, P. F.: TROPOMI on the ESA Sentinel-5 Precursor: A GMES mission for global observations of the

atmospheric composition for climate, air quality and ozone layer applications, Remote Sensing of Environment, 120, 70–83, https://doi.org/10.1016/j.rse.2011.09.027, 2012.

Viatte, C., Strong, K., Paton-Walsh, C., Mendonca, J., O'Neill, N. T., and Drummond, J. R.: Measurements of CO, HCN, and C_2H_6 Total Columns in Smoke Plumes Transported from the 2010 Russian Boreal Forest Fires to the Canadian High Arctic, Atmosphere-Ocean, 51, 522–531, https://doi.org/10.1080/07055900.2013.823373, 2013.

Viatte, C., Strong, K., Walker, K. A., and Drummond, J. R.: Five years of CO, HCN, C₂H₆, C₂H₂, CH₃OH, HCOOH and H₂CO total columns measured in the Canadian high Arctic, Atmos. Meas. Tech., 7, 1547–1570, https://doi.org/10.5194/amt-7-1547-2014, 2014.

Viatte, C., Strong, K., Hannigan, J., Nussbaumer, E., Emmons, L. K., Conway, S., Paton-Walsh, C., Hartley, J., Benmergui, J., and Lin, J.: Identifying fire plumes in the Arctic with tropospheric FTIR measurements and transport models, Atmos. Chem. Phys., 15, 2227–2246, https://doi.org/10.5194/acp-15-2227-2015, 2015.

Viatte, C., Lauvaux, T., Hedelius, J. K., Parker, H., Chen, J., Jones, T., Franklin, J. E., Deng, A. J., Gaudet, B., Verhulst, K., Duren, R., Wunch, D., Roehl, C., Dubey, M. K., Wofsy, S., and Wennberg, P. O.: Methane emissions from dairies in the Los Angeles Basin, Atmos. Chem. Phys., 17, 7509–7528, https://doi.org/10.5194/acp-17-7509-2017, 2017.

Wiedinmyer, C., Akagi, S. K., Yokelson, R. J., Emmons, L. K., Al-Saadi, J. A., Orlando, J. J., and Soja, A. J.: The Fire INventory from NCAR (FINN): a high resolution global model to estimate the emissions from open burning, Geoscientific Model Development, 4, 625–641, https://doi.org/10.5194/gmd-4-625-2011, 2011.

Williams, A. P., Abatzoglou, J. T., Gershunov, A., Guzman-Morales, J., Bishop, D. A., Balch, J. K., and Lettenmaier, D. P.: Observed Impacts of Anthropogenic Climate Change on Wildfire in California, Earth's Future, 7, 892–910, https://doi.org/10.1029/2019EF001210, 2019.

Wilmot, T. Y., Mallia, D. V., Hallar, A. G., and Lin, J. C.: Wildfire plumes in the Western US are reaching greater heights and injecting more aerosols aloft as wildfire activity intensifies, Sci Rep, 12, 12400, https://doi.org/10.1038/s41598-022-16607-3, 2022.

Wunch, D., Wennberg, P. O., Toon, G. C., Keppel-Aleks, G., and Yavin, Y. G.: Emissions of greenhouse gases from a North American megacity: GREENHOUSE GAS EMISSIONS IN LA, Geophys. Res. Lett., 36, n/a-n/a, https://doi.org/10.1029/2009GL039825, 2009.

Wunch, D., Toon, G. C., Blavier, J.-F. L., Washenfelder, R. A., Notholt, J., Connor, B. J., Griffith, D. W. T., Sherlock, V., and Wennberg, P. O.: The Total Carbon Column Observing Network, Phil. Trans. R. Soc. A., 369, 2087–2112, https://doi.org/10.1098/rsta.2010.0240, 2011.

Xu, Q., Westerling, A. L., Notohamiprodjo, A., Wiedinmyer, C., Picotte, J. J., Parks, S. A., Hurteau, M. D., Marlier, M. E., Kolden, C. A., Sam, J. A., Baldwin, W. J., and Ade, C.: Wildfire burn severity and emissions inventory: an example implementation over California, Environ. Res. Lett., 17, 085008, https://doi.org/10.1088/1748-9326/ac80d0, 2022.

Yates, E. L., Iraci, L. T., Singh, H. B., Tanaka, T., Roby, M. C., Hamill, P., Clements, C. B., Lareau, N., Contezac, J., Blake, D. R., Simpson, I. J., Wisthaler, A., Mikoviny, T., Diskin, G. S., Beyersdorf, A. J., Choi, Y., Ryerson, T. B., Jimenez, J. L., Campuzano-Jost, P., Loewenstein, M., and Gore, W.: Airborne measurements and emission estimates of greenhouse gases and other trace constituents from the 2013 California Yosemite Rim wildfire, Atmospheric Environment, 127, 293–302, https://doi.org/10.1016/j.atmosenv.2015.12.038, 2016.

https://doi.org/10.5194/acp-2022-671
Preprint. Discussion started: 14 October 2022

Yokelson, R. J., Goode, J. G., Ward, D. E., Susott, R. A., Babbitt, R. E., Wade, D. D., Bertschi, I., Griffith, D. W. T., and Hao, W. M.: Emissions of formaldehyde, acetic acid, methanol, and other trace gases from biomass fires in North Carolina measured by airborne Fourier transform infrared spectroscopy, J. Geophys. Res., 104, 30109–30125, https://doi.org/10.1029/1999JD900817, 1999.

Zhuang, Y., Fu, R., Santer, B. D., Dickinson, R. E., and Hall, A.: Quantifying contributions of natural variability and anthropogenic forcings on increased fire weather risk over the western United States, 9, 2021.